

ARTICLE

Received 16 Sep 2015 | Accepted 14 Jul 2016 | Published 2 Sep 2016

DOI: 10.1038/ncomms12589

OPEN

Cripto is essential to capture mouse epiblast stem cell and human embryonic stem cell pluripotency

Alessandro Fiorenzano¹, Emilia Pascale¹, Cristina D'Aniello¹, Dario Acampora^{2,3}, Cecilia Bassalart⁴, Francesco Russo⁵, Gennaro Andolfi¹, Mauro Biffoni⁶, Federica Francescangeli⁶, Ann Zeuner⁶, Claudia Angelini⁵, Claire Chazaud⁴, Eduardo J. Patriarca¹, Annalisa Fico¹ & Gabriella Minchiotti¹

Known molecular determinants of developmental plasticity are mainly transcription factors, while the extrinsic regulation of this process has been largely unexplored. Here we identify Cripto as one of the earliest epiblast markers and a key extracellular determinant of the naive and primed pluripotent states. We demonstrate that Cripto sustains mouse embryonic stem cell (ESC) self-renewal by modulating Wnt/ β -catenin, whereas it maintains mouse epiblast stem cell (EpiSC) and human ESC pluripotency through Nodal/Smad2. Moreover, we provide unprecedented evidence that Cripto controls the metabolic reprogramming in ESCs to EpiSC transition. Remarkably, Cripto deficiency attenuates ESC lineage restriction *in vitro* and *in vivo*, and permits ESC transdifferentiation into trophectoderm lineage, suggesting that Cripto has earlier functions than previously recognized. All together, our studies provide novel insights into the current model of mammalian pluripotency and contribute to the understanding of the extrinsic regulation of the first cell lineage decision in the embryo.

¹Stem Cell Fate Laboratory, Institute of Genetics and Biophysics 'A. Buzzati-Traverso', CNR, Via Pietro Castellino 111, 80131 Naples, Italy. ²Institute of Genetics and Biophysics 'A. Buzzati-Traverso', CNR, 80131 Naples, Italy. ³IRCCS Neuromed, 860077 Pozzilli (IS), Italy. ⁴Inserm, UMR1103, F-63001; CNRS, UMR6293, F-63001; Université Clermont Auvergne, Laboratoire GReD, BP 10448, Clermont-Ferrand F-63000, France. ⁵Institute for Applied Mathematics 'Mauro Picone', CNR, 80131, Naples, Italy. ⁶Department of Hematology, Oncology and Molecular Medicine, Istituto Superiore di Sanità, Rome 00161, Italy. Correspondence and requests for materials should be addressed to G.M. (email: gabriella.minchiotti@igb.cnr.it) or to A.F. (email: annalisa.fico@igb.cnr.it).

In mammals, pluripotency is maintained in the inner cell mass (ICM) of early embryo during the formation of epiblast (EPI), which is shielded from extraembryonic differentiation and concomitantly gains the capacity to generate all cell types of the organism. The formation of these lineages results from two subsequent cell fate decisions. The first, occurring at the 16- to 32-cell stage, determines the specification of trophoblast (TE) and ICM; the second cell-fate decision controls the formation of the primitive endoderm (PrE) and EPI within the ICM. The emergence of the pluripotent EPI and PrE lineages within the ICM involves initial co-expression of lineage-associated markers followed by a salt-and-pepper distribution of lineage-biased cells until the time of implantation when cell lineage determination is established^{1,2}. Two distinct states of mouse pluripotency can be captured *in vitro*, that is, embryonic stem cells (ESCs) and EPI stem cells (EpiSCs), which reflect the ground-state naive and the primed EPI, respectively³. Although ESCs grow as packed domed colonies and are stabilized by leukemia inhibitory factor (LIF)/Stat3 signalling, mEpiSCs depend on basic fibroblast growth factor (bFGF) and transforming growth factor- β (TGF β)/Activin signalling and are characterized by a flattened morphology^{4,5}. Mouse EpiSCs can be also generated *in vitro* from ESCs, providing a useful model system to study pluripotent state transition that occurs at implantation⁶. Unlike mouse ESCs, human ESCs (hESCs) depend on TGF β /Activin signalling and share common features of mEpiSCs with respect to growth requirements, morphology, clonogenicity and gene expression patterns³. Mouse ESC (mESC) cultures are not homogeneous but comprise dynamically interchanging subpopulations^{7,8}. This heterogeneity probably reflects the developmental plasticity of the early mouse embryo; however, a mechanistic understanding of this metastability *in vitro* is still far from complete. Specifically, which is the precise correlation of these different pluripotency states with the *in vivo* equivalents is still a question of debate. Known molecular markers of such plasticity are mainly transcription factors operating within a pluripotency gene regulatory network⁹. More recently, metabolites are emerging as key regulators of stem cell plasticity, acting as epigenetic modifiers^{10,11}; however, much less is known on the role of microenvironment. Indeed, elucidation of the extrinsic mechanisms that control stem cell plasticity is crucial for understanding both early embryo development and controlling the differentiation potential of pluripotent stem cells¹². In the attempt to shed lights on this issue, we focused on the glycosylphosphatidylinositol (GPI)-anchored extracellular protein Cripto. Cripto is a key developmental factor and a multifunctional signalling molecule¹³. In the mouse embryo, *Cripto* is essential for primitive streak formation and patterning of the anterior–posterior axis during gastrulation¹⁴ and it negatively regulates ESC neural differentiation while permitting cardiac differentiation¹⁵. Although largely considered as a stem cell surface marker¹⁶, no studies so far have directly investigated its functional role in pluripotency. In this study, we report the consequences of genetic and pharmacological modulation of Cripto signalling on the generation and/or maintenance of mEpiSCs and hESCs.

Results

Cripto heterogeneity in the early blastocyst and ESCs. In the pre-implantation embryo (E3.5), *Cripto* messenger RNA and protein were present in the blastomeres of the ICM in a salt-and-pepper pattern (Fig. 1). Indeed, *Cripto* expression was highly enriched in *Nanog*-expressing cells, whereas it was absent in PrE cells and TE marked by *Cdx2* (Fig. 1a,b)¹⁷. After cell sorting at E4.5, *Cripto* was co-expressed with *Pecam1*, a membrane EPI

marker, but not *Disabled 2*, which labels the PrE (Fig. 1c), as was previously shown^{18,19}. Thus, *in situ* expression analysis revealed that *Cripto* is homogeneously expressed in EPI cells only as early as EPI versus PrE specification occurs within the ICM, earlier than previously reported^{18,19}. *Cripto* remains strongly expressed in the maturing EPI until gastrulation where it becomes restricted to the primitive streak^{14,20}.

To assess whether the heterogeneous distribution of *Cripto* *in vivo* was retained *in vitro*, we analysed *Cripto* protein distribution in serum/LIF ESC cultures⁹. Immunofluorescence and fluorescence-activated cell sorting (FACS) analysis showed a heterogeneous pattern of surface *Cripto* protein expression (Fig. 2a,b) and revealed that ESCs clearly segregated in two cell populations of *Cripto*^{High} and *Cripto*^{Low}, which rapidly returned to the equilibrium under ESC self-renewing conditions (Fig. 2b). Interestingly, *Cripto* expression increased in 2i/LIF culture conditions (Supplementary Fig. 1a), in which ESCs show lower expression of lineage-associated genes and are closer to the pluripotent cells of the ICM^{6,21}. The dynamic equilibrium of distinct functional states in serum ESCs is characterized by the heterogeneous expression of different pluripotency transcription factors, for example, *Nanog*, *Stella* (*Dppa3*) and *Esrrb*. We thus evaluated the expression of pluripotency markers in the *Cripto*^{Low} and *Cripto*^{High} cell populations and found that it was significantly reduced in *Cripto*^{Low} post sorting, whereas it rapidly returned to the equilibrium after *in vitro* culture (Fig. 2c). On the contrary, *Oct4*, which is homogeneously expressed in serum/LIF ESCs²², was expressed at comparable levels in the two subpopulations (Fig. 2c). These data indicated that *Cripto* protein levels dynamically fluctuate in ESCs and correlate with the metastable expression of key pluripotency transcription factors. A similar heterogeneous and fluctuating expression of *Cripto* has been recently described in patient-derived colon cancer stem cells, where *Cripto* positivity oscillates in correspondence to increased stemness states²³, and in a human glioblastoma cell line²⁴. Interestingly, fluctuations of *Cripto* protein levels occurred on small variations of the transcript (Fig. 2c), suggesting that regulation does not primarily occur at a transcriptional level as described in colon cancer stem cells²³.

Decreased self-renewal properties of *Cripto* KO ESCs. To assess the relevance of the correlation between *Cripto* and the expression of pluripotency genes to potency and fate choice, we analysed two independent *Cripto* Knock Out (KO) ESC (KO.1 and KO.2) clones. Similar to that observed in *Cripto*^{Low} and *Cripto*^{High} cell populations, the pluripotency genes were downregulated in both *Cripto* KO ESC clones compared with Control (Fig. 2d). Despite this molecular signature, *Cripto* KO ESCs propagated at high density retained the capacity to form tightly packed dome-shaped colonies. Nevertheless, when *Cripto* KO ESCs were plated at low density in a colony-formation assay, the colonies with a flat morphology and a partial/low alkaline phosphate (AP) staining significantly increased, at the expense of the typical dome-like AP⁺ ESC colonies (Fig. 2e). Interestingly, this phenotype was rescued by the addition of either recombinant Wnt3a (Fig. 2e), which is a key regulator of ESC self-renewal²⁵, or the glycogen synthase kinase 3 inhibitor CHIR99021, a selective inhibitor of β -catenin degradation, as well as in 2i/LIF culture conditions (Fig. 2e and Supplementary Fig. 1b). We thus reasoned that *Cripto* deficiency might affect sensitivity to Wnt signalling and eventually ESC self-renewal *in vitro*. We thus measured Wnt/ β -catenin activity in wild-type (WT) and *Cripto* KO ESCs using the TOP flash/luciferase reporter construct. *Cripto* KO ESCs showed reduced luciferase activity already at baseline conditions, which persisted on stimulation with increasing doses (5–10 ng ml⁻¹) of

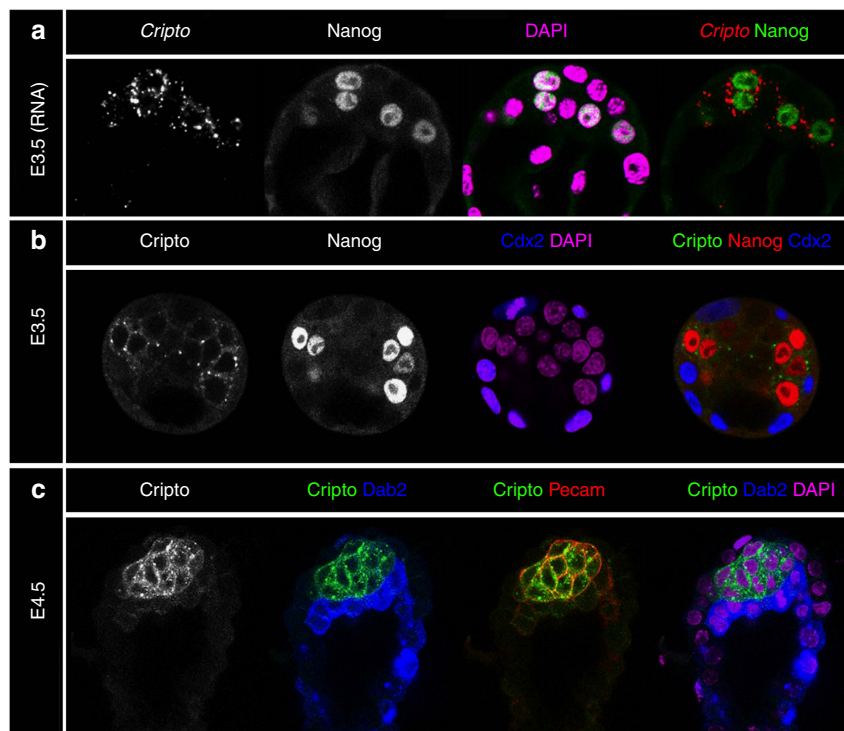


Figure 1 | Cripto is specifically expressed in EPI cells. (a) FISH and (b) immunofluorescence analyses of Cripto expression at E3.5. Both *Cripto* RNA and protein are present in Nanog-expressing cells. (c) By E4.5, *Cripto* remains expressed in the EPI, labelled by Pecam1 and is absent from the PrE revealed by Disabled 2 (Dab2) and the TE.

Wnt3a. On the contrary, addition of high doses of Wnt3a (50 ng ml^{-1}) to WT and Cripto KO ESCs resulted in similar activation of the reporter (Fig. 2f). In line with these findings, Cripto KO ESCs showed decreased levels of nuclear β -catenin, which increased on chemical activation of Wnt/ β -catenin pathway (Supplementary Fig. 1c). Accordingly, expression of the Wnt target gene *Leif1* was downregulated in two independent Cripto KO ESC clones (Supplementary Fig. 1d). Interestingly, Cripto is able to positively modulate Wnt signalling in human mammary epithelial and mouse teratocarcinoma cells, but only on Wnt administration²⁶. Maintenance of ESCs *in vitro* also depends on extracellular signalling by LIF and Bmp4. Stimulation of WT and Cripto KO ESCs with either LIF or Bmp4 resulted in similar increase of the phosphorylation of the intracellular effectors Stat3 and Smad1/5, respectively (Supplementary Fig. 1e). All together, these findings indicate that Cripto genetic ablation reduced ESC self-renewal efficiency in fetal bovine serum (FBS)/LIF but not in 2i/LIF culture conditions²⁷ and suggest that Cripto KO specifically altered Wnt response in ESCs. In line with the idea that *Cripto* KO reduced ESC self-renewal properties, we found substantial differences in the efficiency and latency of Cripto KO ESC-derived teratomas (Fig. 2g) but not in their histological composition (Supplementary Fig. 1f) as previously reported²⁸.

Cripto controls the metabolic switch in ESC \rightarrow EpiSC transition.

Our *in vivo* and *in vitro* findings led us to hypothesize that Cripto may have a functional role in the narrow window in which the cells within the ICM are primed to become EpiSCs. To assess this issue directly, WT and Cripto KO ESCs were treated with bFGF (F) and Activin (A), previously shown to permit *in vitro* EpiSC derivation and maintenance⁶. Control cells developed EpiSCs-like flat-shaped colonies with tightly packed cells and highly positive for the tight-junction protein Claudin6 (ref. 29) (Fig. 3a,b). Conversely, Cripto KO ESCs developed less compacted and

morphologically highly heterogeneous colonies showing large areas of Claudin6-negative cells and increased proliferation (Fig. 3a–c and Supplementary Fig. 2a). Interestingly, surface Cripto protein was expressed at higher levels in WT EpiSCs than in serum/LIF ESCs (Supplementary Fig. 2b) consistent with its *in vivo* expression, which is higher in late blastocyst (Fig. 1b,c). We first verified that Activin and/or FGF signalling were efficiently induced in Cripto KO ESCs (Fig. 3d and Supplementary Fig. 2c) and then performed RNA-sequencing (RNA-Seq) transcriptome profiling of WT and Cripto KO ESC \rightarrow EpiSC transition. As expected, culture conditions of EpiSC induction (F/A) extensively modified the transcriptome of both WT and Cripto KO ESCs, deregulating $\sim 3,000$ protein-coding genes (≥ 2 -fold, posterior probability (PP) ≥ 0.95 ; Supplementary Data 1,2). However, F/A-treated Cripto KO ESCs showed downregulation of both EpiSCs markers (*Fgf5*, *Otx2*, *Cerberus*, *Brachyury* (*Bra*), *Sox17* and *Foxa2*) and the pluripotency genes (*Oct4* and *Nanog*)³⁰ (Fig. 3e). These results were further validated by quantitative PCR (qPCR) analysis using two independent Cripto KO ESC clones, showing that this set of genes were significantly downregulated in both biological replicates (Fig. 3f and Supplementary Fig. 2d). Consistent with these findings, *Cripto* complementary DNA (cDNA) overexpression was able to fully rescue EpiSCs markers' expression in Cripto KO ESC \rightarrow EpiSC transition (Supplementary Fig. 2e,f). Remarkably, immunofluorescence analysis revealed that the number of Nanog-, Oct4-, Otx2-, Foxa2- and Sox17-positive cells were all severely reduced in F/A Cripto KO cells (Fig. 3g and Supplementary Fig. 2g), thus further supporting the idea that ESC \rightarrow EpiSC transition was impaired. Interestingly, besides a set of $\sim 2,300$ ($\sim 70\%$) common genes deregulated in both WT and Cripto KO ESC \rightarrow EpiSC transition, we identified two different sets of genes that were uniquely deregulated (Fig. 4a and Supplementary Data 3). Specifically, Gene Ontology (GO) analysis showed that a large cluster of genes coding for

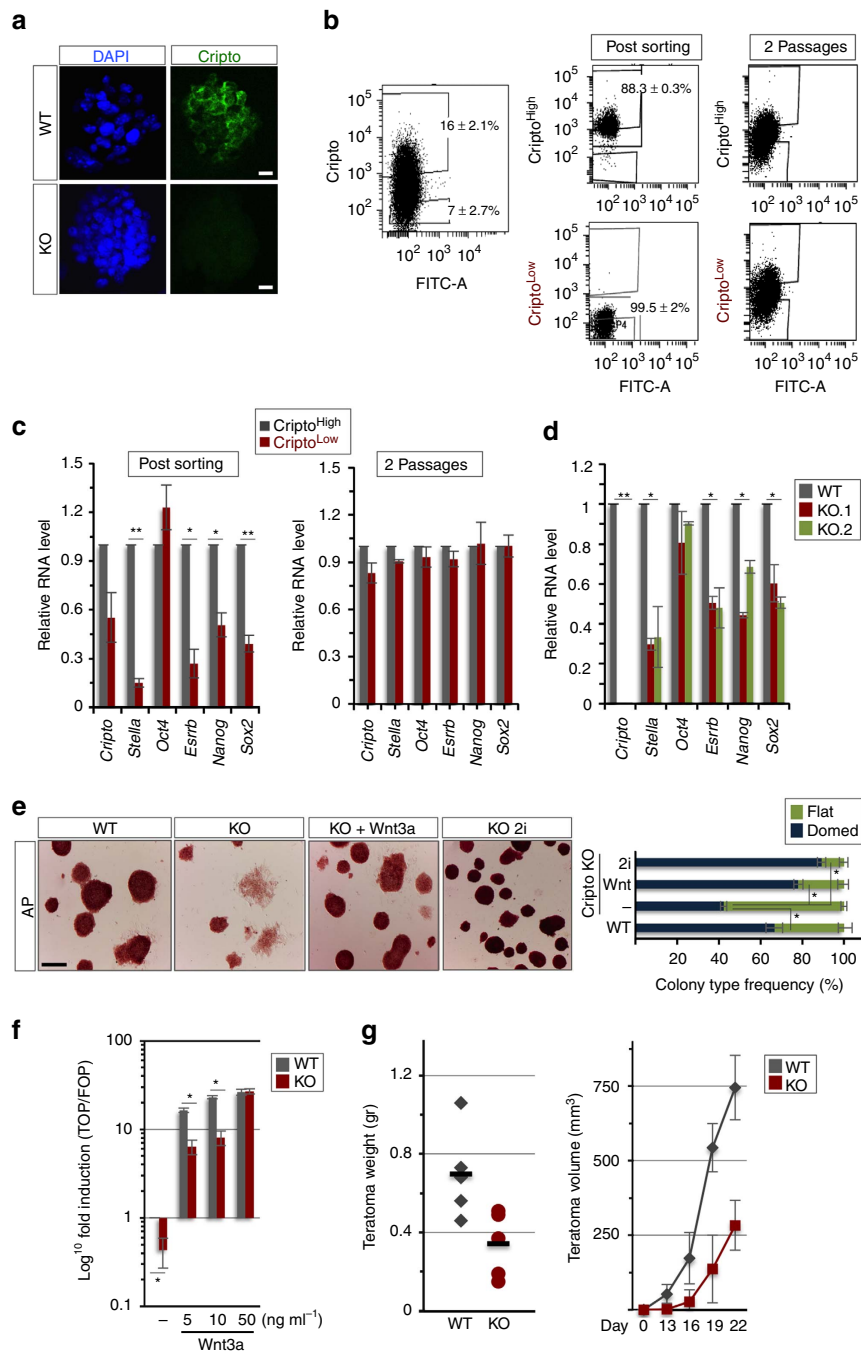


Figure 2 | Cripto sustains mESC self-renewal by modulating canonical Wnt signalling. (a) Immunofluorescence of Cripto on non-permeabilized WT and Cripto KO ESCs. Nuclei were stained with 4,6-diamidino-2-phenylindole (DAPI). Scale bar, 75 μ m. (b) FACS-based separation of Cripto^{High} and Cripto^{Low} in serum/LIF mESCs. Data are mean \pm s.e.m. ($n = 3$). (c) qPCR of Cripto and pluripotency genes' expression on Cripto^{High} and Cripto^{Low} cells immediately after sorting and after two passages in culture. Relative RNA level was normalized to *Gapdh*; data are mean \pm s.e.m. ($n = 3$; * $P < 0.01$ and ** $P < 0.005$). (d) qPCR of pluripotency genes' expression in WT and two independent Cripto KO ESC clones (KO.1 and KO.2) in serum/LIF culture conditions. Relative RNA level was normalized to *Gapdh*; data are mean \pm s.e.m. ($n = 3$; * $P < 0.01$ and ** $P < 0.005$). (e) Representative pictures (scale bar, 100 μ m) of AP-stained and colony-type frequency (domed versus flat) of colonies generated from WT, Cripto KO, KO + Wnt3a (50 ng ml⁻¹) and KO 2i ESCs, at day 6 after plating (~ 100 colonies scored per condition). (f) TOP flash reporter activation in WT and Cripto KO ESCs in baseline conditions and following Wnt3a stimulation at indicated concentrations. Data are mean \pm s.e.m. ($n = 3$); * $P < 0.01$. (g) Effect of Cripto depletion on teratomas formation. Quantitative analysis of tissue weights (left panel) and temporal kinetic analysis (right panel) of teratomas growth (volume, mm³). Data are mean \pm s.e.m. (five mice per group).

components of the five respiratory electron transport complexes, which are involved in mitochondrial oxidative phosphorylation, were downregulated only in WT ESC \rightarrow EpiSC transition (P -value = 1.2×10^{-19}), whereas their expression was unvaried in

Cripto KO (Fig. 4b,c). Interestingly, one of the earliest events in the ESC \rightarrow EpiSC transition is a dramatic metabolic switch, which converts a bivalent ESC metabolism to an exclusively glycolytic EpiSC metabolism³¹. To assess whether this metabolic

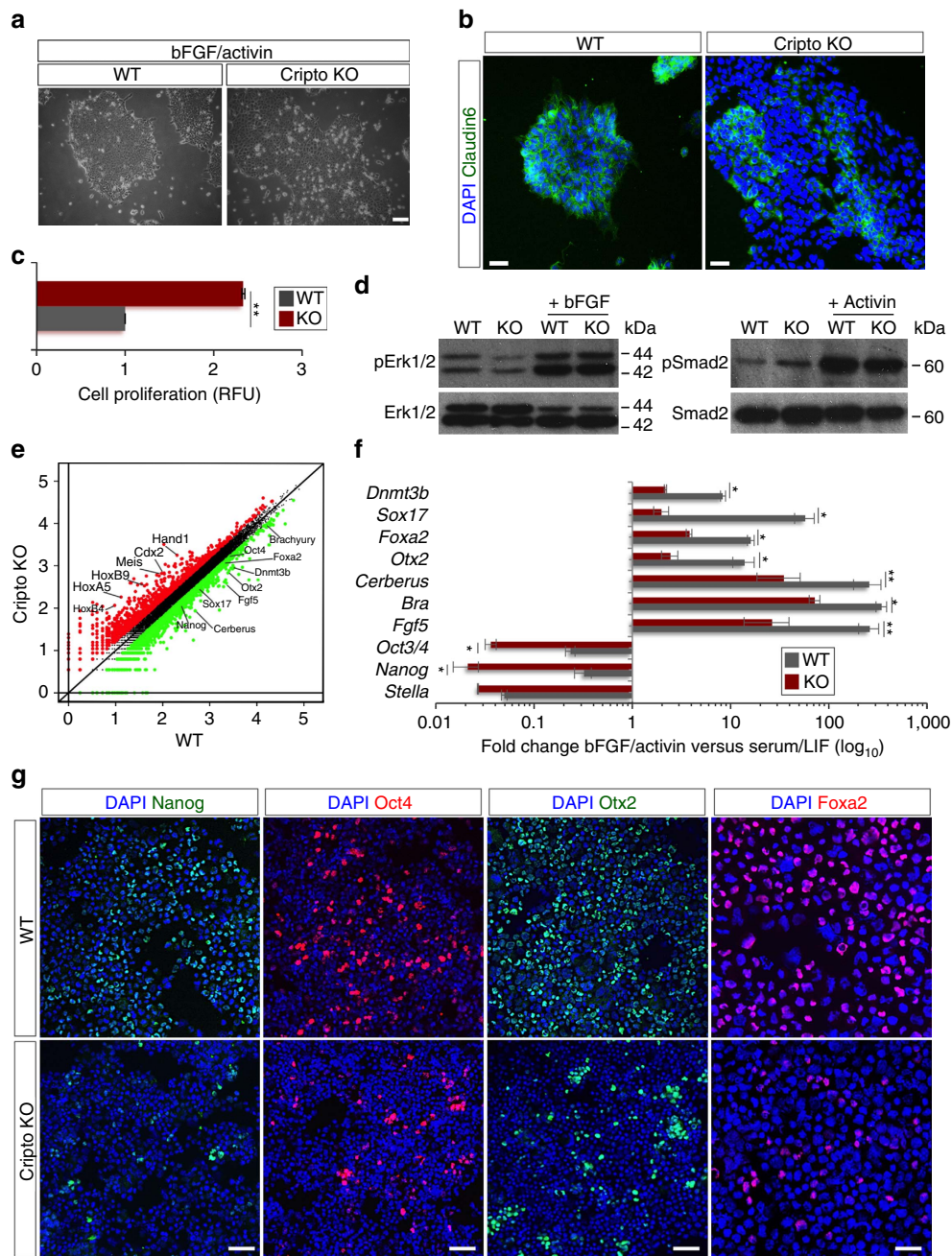


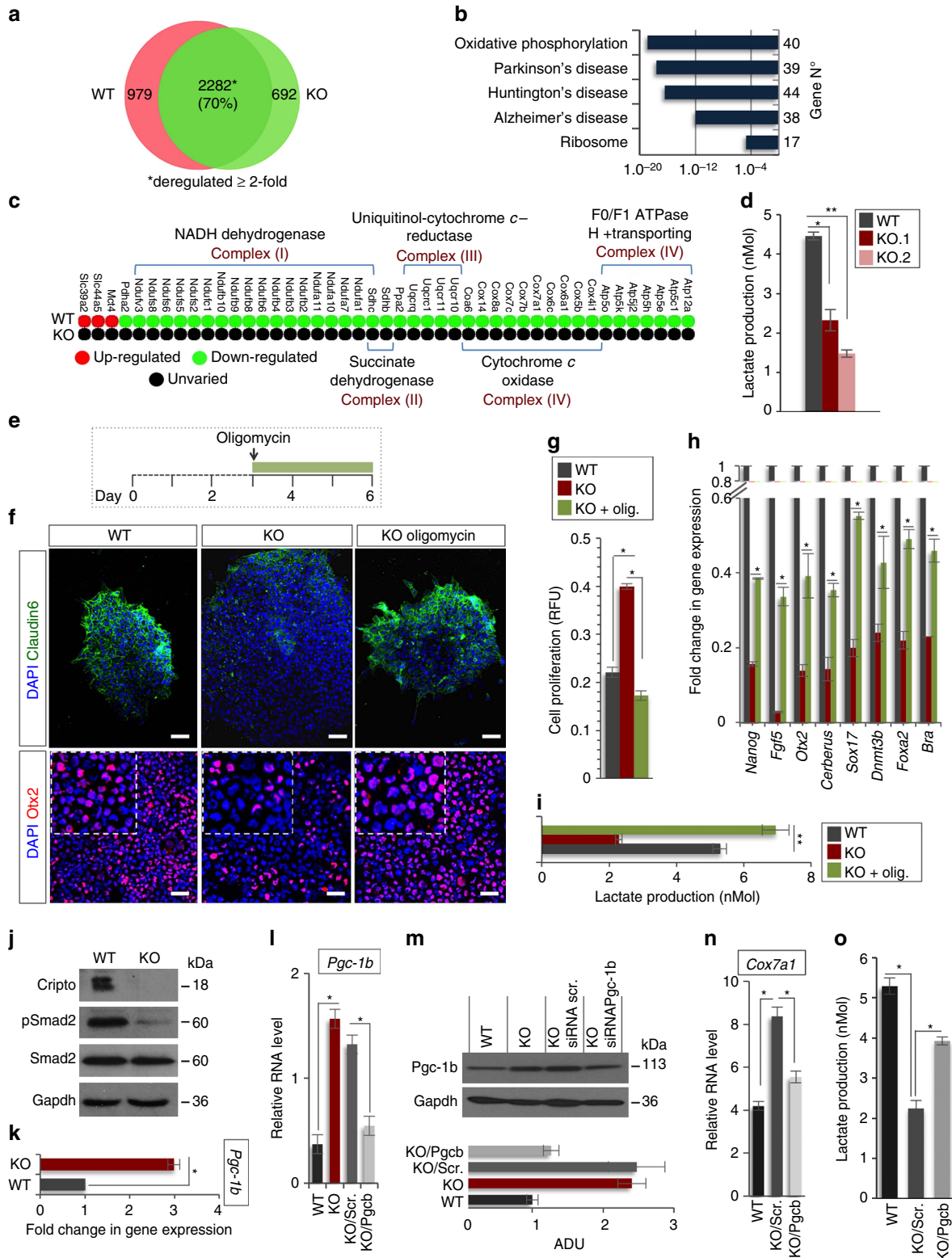
Figure 3 | Cripto genetic ablation prevents ESC→EpiSC transition. (a) Representative photomicrographs of FGF/Activin (F/A) WT and Cripto KO cell colonies (scale bar, 100 μm). (b) Immunofluorescence of Claudin6 in F/A WT and Cripto KO cell colonies (scale bar, 75 μm). (c) Proliferation of F/A WT and Cripto KO cells measured by the CyQuant assay and expressed as relative fluorescence units (RFU). Data are mean ± s.e.m. (n = 3; **P < 0.005). (d) Western blot analysis of WT and Cripto KO ESCs' response to bFGF and Activin, using pErk1/2, Erk1/2, pSmad2 and Smad2 antibodies. (e) Scatter plot of RNA-seq data shows differentially expressed genes in F/A Cripto KO versus WT cells. The black circles delineate the boundaries of <2-fold difference in gene expression levels. Genes showing a higher or lower expression level (log₁₀ FC > 0.2) in Cripto KO versus WT are indicated as red and green circles, respectively. (f) Effect of F/A on the expression of selected markers in WT and Cripto KO ESCs. Data are expressed as fold change of EpiSCs (F/A) versus ESCs (serum/LIF) after normalization to *Gapdh* and are mean ± s.e.m. (n = 3; *P < 0.01 and **P < 0.005). (g) Representative pictures of Nanog, Oct4, Otx2 (scale bar, 100 μm) and Foxa2 (scale bar, 75 μm) immunostaining in cytopspinned F/A WT and Cripto KO cells. Nuclei were stained with 4,6-diamidino-2-phenylindole (DAPI).

reprogramming was affected in Cripto KO ESC→EpiSC transition, we measured lactate production as an indicator of the glycolytic activity in F/A WT and Cripto KO cells, from two independent Cripto KO ESC clones (KO.1 and KO.2), and found that it was significantly reduced in Cripto KO compared with Control (Fig. 4d). To evaluate whether this failure to undergo metabolic reprogramming leads to the mutant phenotype, we

asked whether inhibition of oxidative phosphorylation by the mitochondrial ATP synthase inhibitor oligomycin³² could rescue F/A-induced Cripto KO EpiSCs (Fig. 4e–i). Interestingly, F/A-treated Cripto KO ESCs generated tightly packed EpiSCs-like colonies in the presence of oligomycin, with reduced proliferation rates and large areas of Claudin6-positive cells (Fig. 4e–g). Furthermore, oligomycin treatment fully rescued lactate

production (Fig. 4i) and induced the expression of EpiSCs markers (Fig. 4f,h), thus demonstrating that Cripto-dependent metabolic reprogramming is crucial to induce an EpiSC state. To get mechanistic insights into how Cripto acts to regulate this metabolic reprogramming, we focused on the Activin/Nodal/Pgcb axis, which has been recently identified as key regulator of this metabolic switch³¹. Specifically, Activin/Nodal signalling actively represses mitochondrial genes' expression/activity through

inhibition of *Pgc-1b*^{31,33}. Given the key role of Cripto as positive Nodal co-receptor³⁴, we hypothesized that a Cripto/Nodal/Pgcb axis may control mitochondrial gene expression/activity and eventually regulate the metabolic reprogramming in ESC→EpiSC transition. In line with this hypothesis, Smad2 phosphorylation was reduced in F/A Cripto KO cells compared with Control (Fig. 4j), whereas *Pgc-1b* expression was significantly upregulated (Fig. 4k). We then went on and knocked down



Pgc-1b expression in Cripto KO ESC→EpiSC transition by transient transfection of small interfering RNAs at the same time point as in oligomycin treatment (Fig. 4e). Remarkably, *Pgc-1b* downregulation (Fig. 4l,m) repressed *Cox7a1* mitochondrial gene expression (Fig. 4n) and increased lactate production (Fig. 4o). All together, these results provide unprecedented evidence that Cripto regulates the metabolic reprogramming that is crucial for ESC to EpiSC conversion and suggest that it occurs, at least in part, through activation of the Nodal/*Pgc-1b*/mitochondrial genes axis.

Cripto deficiency attenuates ESC lineage restriction. Our findings that Cripto is required for ESC→EpiSC transition leave open the question of the fate of F/A-induced Cripto KO ESCs. To address this issue, we first analysed the ~700 genes that were uniquely deregulated in Cripto KO ESC→EpiSC transition (Fig. 4a). Interestingly, GO analysis revealed a consistent over-representation of genes in the Kyoto Encyclopedia of Genes and Genomes (KEGG) pathway related to pattern specification processes/formation (Supplementary Fig. 3a). Strikingly, this includes a large set of *Hox* genes that were uniquely upregulated in Cripto KO (Supplementary Fig. 3b,c), indicating cell differentiation. Furthermore, we focused our attention on *Cdx2* and *Hand1* genes (Fig. 3e), which are involved in trophoblast lineage specification and differentiation with *Msx2* (ref. 17), and first confirmed that they were all significantly upregulated in Cripto KO transition by qPCR analysis (Fig. 5a)¹⁷. In line with RNA expression data, the percentage of *Cdx2*-positive cells almost doubled in F/A Cripto KO cells compared with Control as indicated by FACS analysis (*Cdx2*⁺ cells 2.6 ± 0.9% WT versus 14.5 ± 3.1% KO; Supplementary Fig. 3d). To further characterize these *Cdx2*-positive cell population, we performed double staining with *Cdx2* and various markers on two independent Cripto KO ESC clones (KO.1 and KO.2). First, consistent with the idea that *Cdx2* plays a central role in blastocyst development by repressing the pluripotency gene *Oct4* (ref. 17), *Cdx2*-positive cells did not express *Oct4* (Fig. 5b and Supplementary Fig. 3e). To assess whether *Cdx2* was labelling posterior mesoderm rather than TE³⁵, we performed double staining with *Cdx2* and *Brachyury* (Fig. 5b and Supplementary Fig. 3e). Interestingly, quantification of *Cdx2* + / *Brachyury* ± cells showed that the majority of *Cdx2*-positive cells did not express *Brachyury* (Fig. 5c). Finally, consistent with the idea that Cripto deficiency was promoting an extraembryonic fate, we found that *Cdx2*-positive cells also expressed the trophoblast marker *Gata3* (ref. 36, Fig. 5b and Supplementary Fig. 3e). Interestingly, it has been recently shown that *Smad2*

represses autocrine bone morphogenetic protein (BMP) signalling, which eventually leads to TE differentiation³⁷. Remarkably, while *Smad2* phosphorylation was reduced in F/A Cripto KO cells compared with Control (Fig. 4j), BMP-dependent *Smad1/5* phosphorylation was induced (Fig. 5d), suggesting that this is the mechanism underlying Cripto deficiency-induced TE differentiation. On the contrary, extracellular signal-regulated kinase (ERK) signalling was unaffected (Fig. 5d). To further determine the differentiation capacities of Cripto KO ESCs towards the trophoblast lineage, we subjected WT and Cripto KO ESCs to culture conditions that favour trophoblast stem cell (TSC) differentiation³⁸. Both WT and Cripto KO ESCs developed dense undifferentiated colonies (Fig. 5e) and expression analysis revealed a strong upregulation of trophoblast lineage determinants *Cdx2*, *Gata3*, *Eomes*, *Tead4* and *Elf5*, which were significantly higher in Cripto KO versus WT TSC cultures. Conversely, expression of the pluripotency genes *Cripto*, *Oct4* and *Nanog* was strongly reduced (Fig. 5f and Supplementary Fig. 3f). The upregulation of *Cdx2* and *Eomes* in Cripto KO cultures was confirmed by immunofluorescence (Fig. 5e and Supplementary Fig. 3g) and FACS analysis (*Cdx2*⁺ cells 8.9 ± 0.2% WT versus 28.8 ± 3.7% KO; Fig. 5g). All together, these results indicated that TSC differentiation was induced more efficiently in Cripto KO ESCs. Intriguingly, cells with a morphology characteristic of trophoblast giant cells were observed in Cripto KO but not in WT cultures (Fig. 5e), leading to speculate that these cells were undergoing spontaneous trophoblast differentiation. Interestingly, this is consistent with previous findings that *Nodal* is required to sustain the TSC stemness and inhibit their precocious differentiation *in vivo*³⁹.

To further explore this phenotype, we assessed the capacity of Cripto KO ESCs to contribute to TE *in vivo*. To this end, green fluorescent protein (GFP)-labelled WT and Cripto KO ESCs were microinjected into morulas and the resulting blastocysts were examined. Both WT and Cripto KO ESCs efficiently contributed to the ICM. Interestingly, Cripto KO ESCs also colonized the TE⁴⁰, whereas, as expected, WT ESCs did not contribute to this extraembryonic lineage (Fig. 6a,b). Accordingly, whole-mount immunostaining for the trophoblast marker *Cdx2* and the ICM marker *Oct4* showed that Cripto KO-GFP ESCs in the TE expressed *Cdx2*, whereas GFP co-localized with *Oct4* in the ICM of both WT and Cripto KO chimeric blastocysts (Fig. 6a). To further assess the developmental plasticity of Cripto KO ESCs in the embryonic context and evaluate their contribution to the extraembryonic tissue, injected morulas were implanted into foster mothers and chimeric embryos were analysed at E6.5 (Fig. 6c). None of the scored Cripto KO-GFP chimeric embryos

Figure 4 | Cripto controls the metabolic reprogramming in ESC→EpiSC transition. (a) Venn diagram of genes differentially expressed (≥2-fold) or uniquely deregulated in Cripto KO versus WT ESC→EpiSC transition. (b) GO analysis (<http://david.abcc.ncifcrf.gov>) of protein coding genes (979) uniquely deregulated in WT ESC→EpiSC showing gene enrichment in KEGG Pathway. (c) Heatmap of genes involved in oxidative phosphorylation in WT and Cripto KO ESC→EpiSC transition. (d) Lactate concentration of F/A WT and Cripto KO cells. Two independent Cripto KO ESCs (KO.1 and KO.2) were used. Data are mean ± s.e.m. ($n = 3$; * $P < 0.01$ and ** $P < 0.005$). (e) Schematic representation of the experimental procedure. (f) Representative immunofluorescence of *Claudin6* and *Otx2* in F/A WT, Cripto KO and Cripto KO + oligomycin colonies and cytopinned cells (scale bar, 75 μm). Inserts are higher magnification images of selected areas. (g) Proliferation of F/A WT, Cripto KO and Cripto KO + oligomycin cells measured by the CyQuant assay and expressed as relative fluorescence units (RFU). Data are mean ± s.e.m. ($n = 3$; * $P < 0.01$). (h) qPCR of selected markers in F/A WT, Cripto KO and Cripto KO + oligomycin. Relative RNA level was normalized to *Gapdh*; data are mean ± s.e.m. ($n = 3$; * $P < 0.01$). (i) Lactate concentration of F/A WT, Cripto KO and Cripto KO + oligomycin cells. Data are mean ± s.e.m. ($n = 3$; ** $P < 0.005$). (j) Western blot analysis of Cripto and p-Smad2 in F/A WT and Cripto KO cells. *Smad2* and *Gapdh* were loading controls. (k) qPCR of *Pgc-1b*. Data are fold induction of Cripto KO versus WT F/A after normalization to *Gapdh* and are mean ± s.e.m. ($n = 3$; * $P < 0.01$). (l) qPCR of *Pgc-1b* on F/A WT and Cripto KO cells transfected with two independent *Pgc-1b* small interfering RNAs (siRNAs) (KO/siPgc) or control siRNA (KO/Scr.) at day 3 during ESC→EpiSC. Data are fold induction of Cripto KO versus WT and KO/Scr. versus KO/Pgc after normalization to *Gapdh* and are mean ± s.e.m. ($n = 3$; * $P < 0.01$). (m) Western blot analysis of *Pgc-1b* in F/A WT, Cripto KO, Cripto KO/Scr. and Cripto KO/siPgc-1b (KO/Pgc). *Gapdh* were loading controls. The densitometric analysis is expressed in arbitrary unit (ADU) as the *Pgc-1b*/*Gapdh* ratio. Data are mean ± s.e.m. ($n = 2$). (n) qPCR of *Cox7a1* and (o) lactate concentration in culture medium of F/A WT, Cripto KO/Scr and Cripto KO/Pgc. Relative RNA level was normalized to *Gapdh*. Data are mean ± s.e.m. ($n = 3$; * $P < 0.01$).

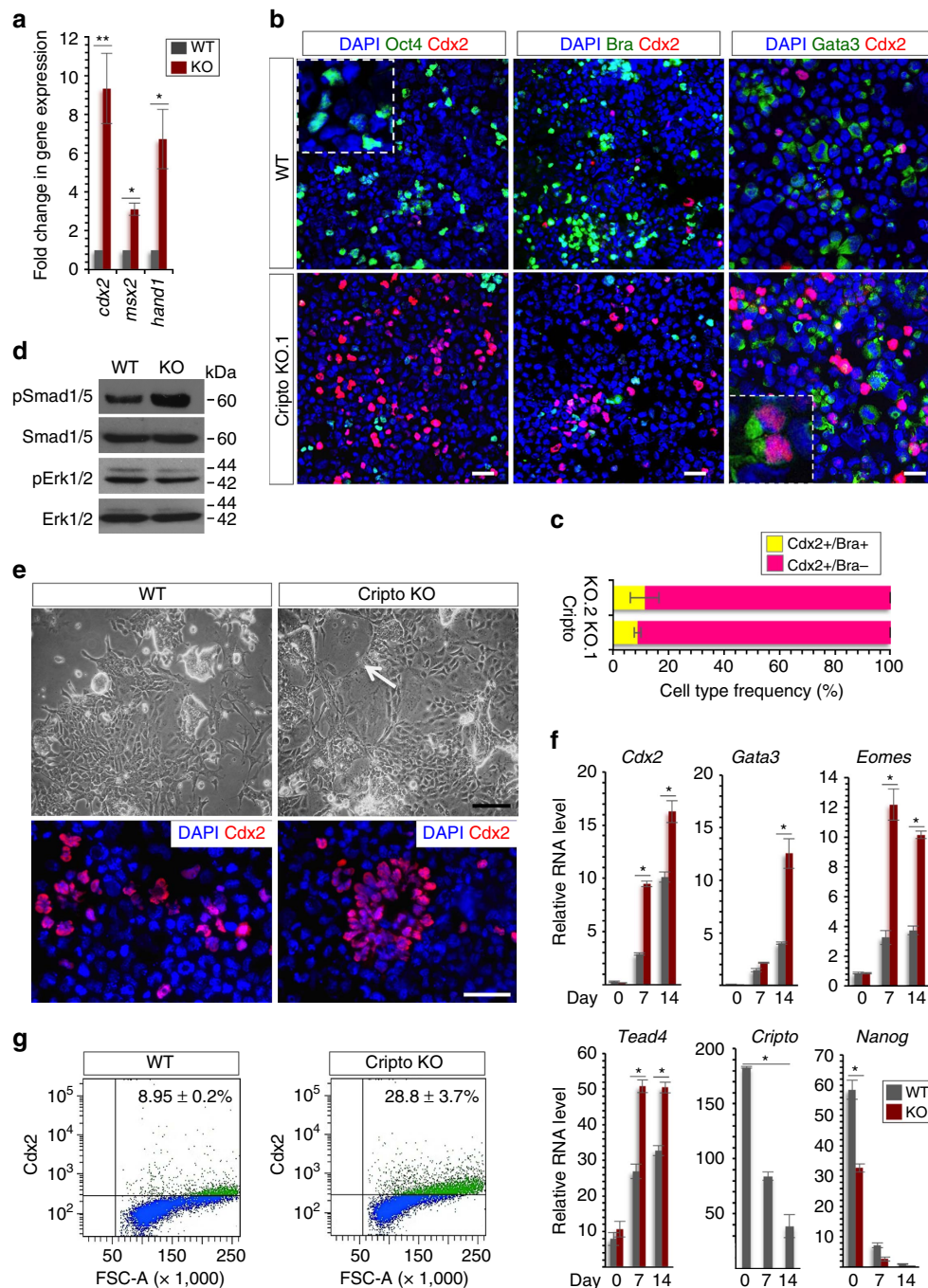


Figure 5 | Cripto depletion attenuates ESC differentiation potential towards embryonic lineages *in vitro*. (a) qPCR analysis of *Cdx2*, *Msx2* and *Hand1* trophoblast markers in WT and Cripto KO ESC → EpiSC transition (day 6). Data are shown as fold change compared with ESCs after normalization to *Gapdh* and are mean ± s.e.m. ($n = 3$; $*P < 0.01$). (b) Representative pictures of Oct4/Cdx2, Bra/Cdx2 and Gata3/Cdx2 double immunostaining of F/A WT and Cripto KO (clone KO.1) cytospinned cells. Inserts are higher magnification images of selected areas. Nuclei were stained with 4,6-diamidino-2-phenylindole (DAPI). Scale bar, 75 μ m. (c) Quantification of Cdx2 + /Brachyury ± cells distribution. Data are expressed as percentage over total number of Cdx2 + cells ($n \approx 300$) on two independent Cripto KO ESC clones (KO.1 and KO.2) and are mean ± s.e.m. ($n = 3$). (d) Western blot analysis of pSmad1/5 and pErk1/2 protein levels in F/A WT and Cripto KO cells. Smad1/5, Erk1/2 were used as loading controls. (e) Photomicrographs of TSC colonies (top panels) and Cdx2 immunostaining in cytospinned cells (bottom panels) (scale bar, 75 μ m) generated by WT and Cripto KO ESCs. White arrow indicates a trophoblastic giant cell (scale bar, 100 μ m). (f) qPCR analysis of TE and pluripotency markers at different time points of WT and Cripto KO TSC differentiation. Relative RNA level was normalised to *Gapdh*; data are mean ± s.e.m. ($n = 3$; $P^* < 0.01$). (g) FACS-based quantification of Cdx2-positive cells at 2 weeks of ESC to TSC differentiation. Data are mean ± s.e.m. ($n = 3$).

($n = 25$) showed contribution to the extraembryonic ectoderm or to the ectoplacental cone; however, they showed contribution to the EPI and were phenotypically WT (Fig. 6c). Of note, we hypothesized that Cripto KO cells have a propensity to rapidly

differentiate into giant cells (Fig. 5e) and this could explain why these cells cannot be maintained within the chimeras. This result can also be explained by a non-cell autonomous contribution of Cripto in the WT environment⁴¹. To address this hypothesis, WT

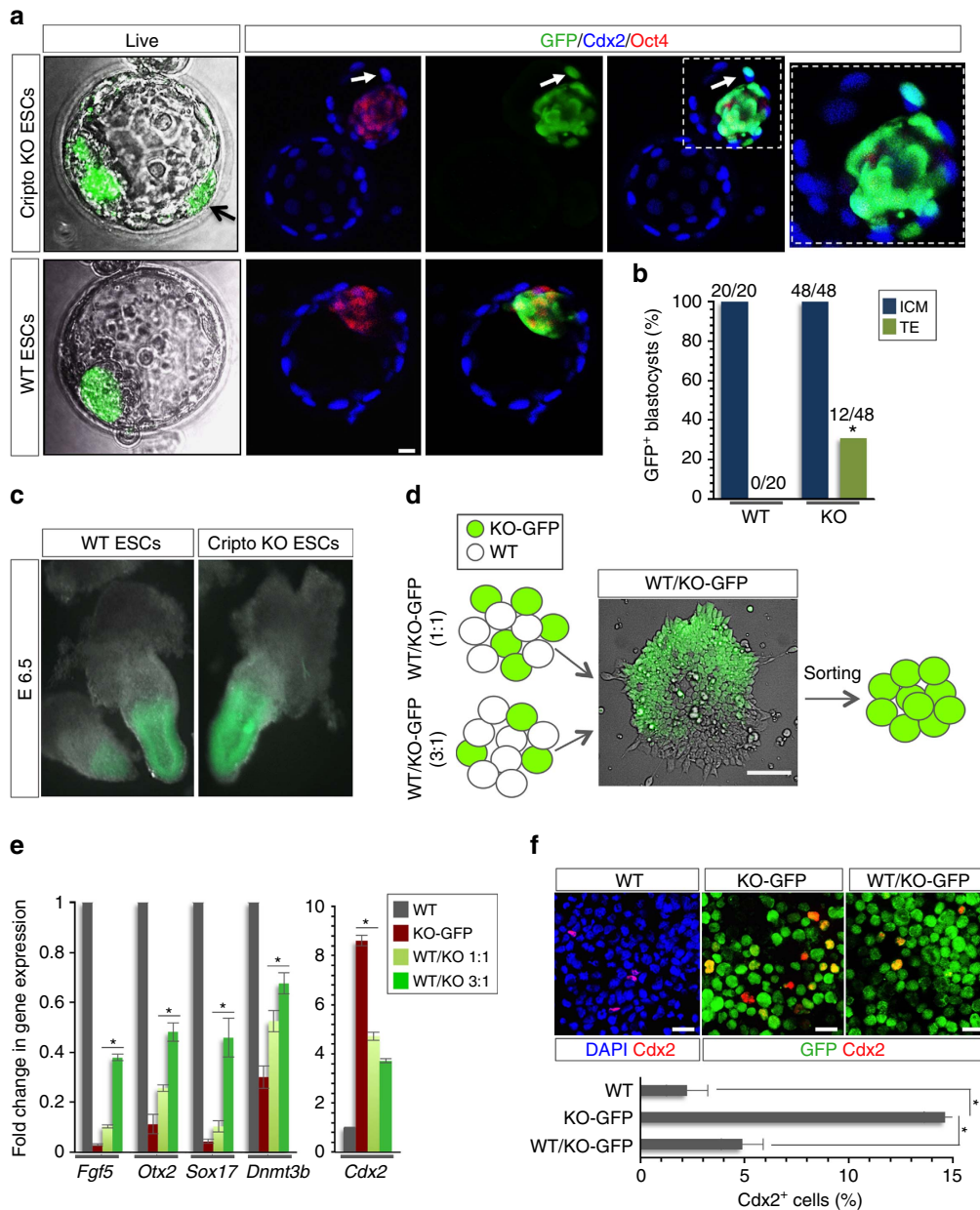


Figure 6 | Cripto depletion attenuates ESC differentiation potential towards embryonic lineages *in vivo*. (a) Chimeric blastocysts from GFP-labelled WT and Cripto KO ESCs by live confocal microscopy imaging (original magnification $\times 20$) and whole-mount immunostaining against GFP, Cdx2 and Oct4; arrow marks GFP⁺ TE cells (scale bar, 10 μ m). (b) Frequency of blastocysts with GFP⁺ ICM and TE cells from WT (blastocysts $n = 20$) and Cripto KO (blastocysts $n = 48$) ESCs. Fisher’s exact test $*P < 0.05$. (c) Representative pictures by AXIOZoom.V16 Zeiss microscopy (original magnification $\times 10$) of chimeric embryos from GFP-labelled WT and Cripto KO ESCs injected into morula and dissected at E6.5. (d) Schematic representation of the experimental procedure and representative picture of co-culture WT and Cripto KO colony. (e) Effect of F/A on the expression of selected markers in WT, Cripto KO ESCs and WT ESCs mixed at 1:1 and 3:1 ratios with Cripto KO-GFP ESCs. Relative RNA level was normalized to *Gapdh*; data are mean \pm s.e.m. ($n = 3$; $P^* < 0.01$). (f) Representative pictures of 4,6-diamidino-2-phenylindole (DAPI)/Cdx2 and GFP/Cdx2 double immunostaining (upper panels; scale bar, 75 μ m) and quantification of Cdx2⁺ cells (bottom panel; ~ 100 cells per condition) of F/A WT, Cripto KO and WT/Cripto KO cytopspinned cells mixed at 3:1 ratio. Data are mean \pm s.e.m. ($n = 3$; $P^* < 0.01$).

ESCs were mixed at different ratios with Cripto KO-GFP ESCs (1:1 and 3:1). Interestingly, at each ratio F/A-treated Cripto KO ESCs generated tightly packed EpiSCs-like colonies similar to that of WT F/A EpiSCs, suggesting that co-culture with WT ESCs rescued the mutant phenotype (Fig. 6d). To further explore this phenotype, F/A Cripto KO-GFP cells were flow-sorted by using the GFP reporter (Supplementary Fig. 4) and assayed separately for EpiSC and TE factors. In line with our hypothesis, expression of EpiSC markers was induced in a dose-dependent manner,

concomitant with a downregulation of *Cdx2* expression (Fig. 6e), which was confirmed by immunofluorescence (Fig. 6f). All together, our data support a model wherein Cripto deficiency affects ESC \rightarrow EpiSC transition and attenuates the normal restriction of ESCs towards embryonic tissue.

Cripto/Nodal sustains mEpiSC and hESC self-renewal. To get further mechanistic insights into the role of Cripto in the

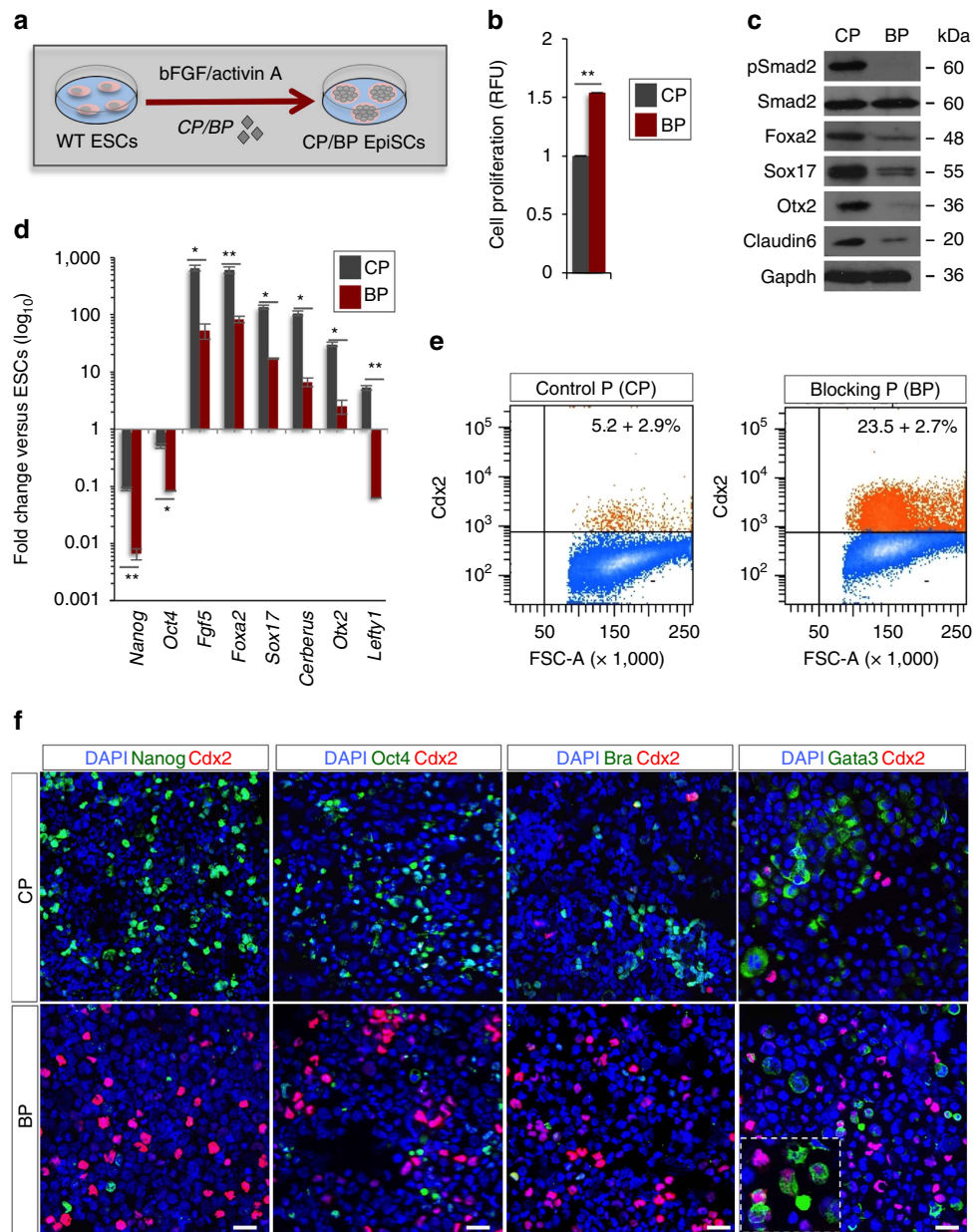


Figure 7 | Pharmacological inhibition of Cripto signalling prevents ESC \rightarrow EpiSC transition. (a) Schematic representation of the experimental procedure. (b) Proliferation of CP/BP-treated cells measured by the CyQuant assay and expressed as RFU. (c) Western blot analysis of pSmad2, Foxa2, Sox17, Otx2 and Claudin6 in CP/BP-treated F/A cells. Smad2 and Gapdh were used as a loading control. (d) Gene expression profiles of selected markers in CP/BP-treated F/A EpiSCs. Data are shown as fold change compared with ESCs (serum/LIF) after normalization to *Gapdh* and are mean \pm s.e.m. ($n=3$; * $P<0.01$ and ** $P<0.005$). (e) FACS quantification of Cdx2⁺ cells in CP/BP-treated cultures. Data are mean \pm s.e.m. ($n=3$). (f) Representative pictures of Nanog/Cdx2, Oct4/Cdx2, Bra/Cdx2 and Gata3/Cdx2 double immunostaining of CP/BP-treated cytopinned cells (scale bar, 75 μm). Inserts are higher magnification images of selected areas. Nuclei were stained with 4,6-diamidino-2-phenylindole (DAPI).

establishment of primed pluripotency, we exploited the activity of a Cripto/ALK-4 blocking peptide (BP), which binds Cripto and antagonizes Cripto/ALK-4 interaction⁴² (Fig. 7a). Although control peptide (CP)-treated F/A ESCs developed EpiSCs-like colonies, Cripto BP-treated cells raised colonies containing highly proliferating and morphologically heterogeneous cell populations (Fig. 7b). As expected, Smad2 phosphorylation was reduced in Cripto BP-treated cells (Fig. 7c), concomitant with the downregulation of EpiSC markers and the pluripotency genes (Fig. 7c,d), as well as upregulation of TE markers (Supplementary Fig. 3h). Furthermore, similar to that observed in F/A-induced Cripto KO cells, Cdx2-positive cells strongly increased in the

presence of Cripto BP (Fig. 7e,f). Interestingly, these Cdx2-positive cells did not express Oct4 and Nanog, and few of them stained positive for the mesoderm marker Brachyury, which in turn was downregulated (Fig. 7f). Finally, we found co-expression of Cdx2 with the trophoblast marker Gata3. All together, these data demonstrate that Cripto/ALK-4/Nodal signalling is required for ESC \rightarrow EpiSC transition and to restrict ESC differentiation potential towards embryonic tissues.

We then asked whether Cripto signalling was required to maintain EpiSC self-renewal. To this end, F/A WT EpiSCs were analysed after subsequent passages in culture in the presence of Cripto CP or BP (Fig. 8a). Although CP-treated EpiSCs developed

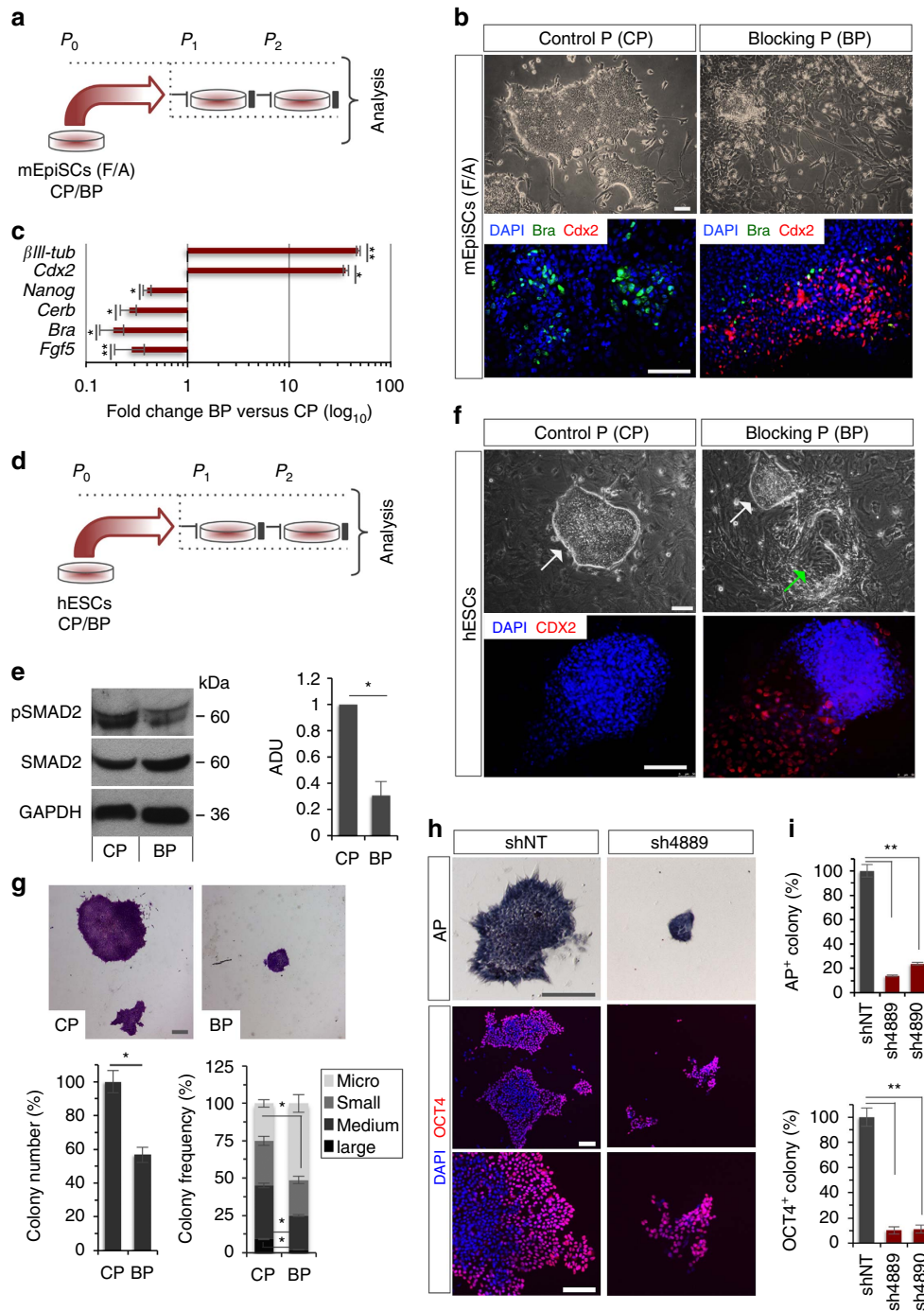


Figure 8 | Cripto is required for maintenance of mouse and human primed pluripotent stem cell states. (a) Schematic representation of the experimental procedure. (b) Representative photomicrographs of brightfield (scale bar, 100 μm) CP/BP-treated F/A EpiSCs colonies (top panels) and immunostaining detection of Bra/Cdx2 (bottom panels) in F/A EpiSCs, after two passages with CP/BP. Nuclei were stained with 4,6-diamidino-2-phenylindole (DAPI). (c) qPCR analysis of EPI-associated (*Fgf5*, *Brachyury* (*Bra*), *Cerberus* (*Cer*) and *Nanog*), trophoblast (*Cdx2*) and neural (*βIII-tubulin*) markers in BP/CP-treated F/A mEpiSCs. Data are expressed as fold change of BP versus CP after normalization to *Gapdh* and are mean ± s.e.m. (n = 3; *P < 0.01 and **P < 0.005). (d) Schematic representation of the experimental procedure. hESCs were passaged either on feeder layer or in Matrigel/feeder-free conditions and in the presence of CP/BP. (e) Western blot analysis of pSMAD2 protein levels in CP/BP-treated hESCs (1 week). SMAD2 and GAPDH were used as loading controls. The densitometric analysis is expressed in arbitrary unit (ADU) as the pSMAD2/SMAD2 ratio. (f) Representative phase contrast pictures (upper panels) of CP/BP-treated hESC colonies after two passages on feeder layer. White and green arrows indicate undifferentiated and differentiated colonies, respectively. Representative picture of CDX2 immunostaining (lower panels) in CP- and BP-treated hESCs. Nuclei were stained with DAPI. Scale bars, 100 μm. (g) Clonogenic assay of hESCs treated with CP and BP for two passages on Matrigel-coated plates. Representative pictures of CP- and BP-treated hESC colonies, stained with crystal violet (top panels). Scale bar, 200 μm. Colony number (bottom left panel) and phenotype frequency (bottom right panel). Data are mean ± s.e.m. (≈ 100 colonies scored/condition; *P < 0.01). (h) Representative photomicrographs of hESC colonies derived from shNT Control and sh4889 *CRIPTO* KD hESCs, and stained for AP (top panels; scale bar, 200 μm) or OCT4 (bottom panels; scale bar, 100 μm). (i) Quantification of AP⁺ (top panel) and OCT4⁺ (bottom panel) colonies. The number of AP⁺ and OCT4⁺ colonies is shown as percentage over shNT hESCs. Data are mean ± s.e.m. (n = 3; **P < 0.005).

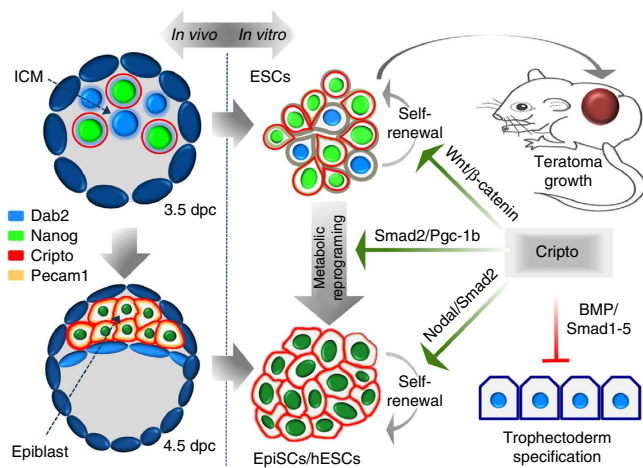


Figure 9 | Schematic summary of Cripto activity in naive and primed pluripotent stem cell states.

Cripto is one of the earliest EPI markers. Cripto-positive cells display a salt-and-pepper distribution and co-localize with Nanog-positive cells (light green) within the ICM of the pre-implantation blastocyst (E3.5). Next, *Cripto* expression becomes homogeneous in the late blastocyst (E4.5), marking all the cells of the EPI (dark green), whereas it is absent in both the TE (dark blue) and in the PrE (light blue). In mouse ESCs, surface Cripto is heterogeneous and highly dynamic and correlates with high levels of pluripotency markers. Moreover, Cripto regulates mouse ESC self-renewal by positively modulating the canonical Wnt/ β -catenin pathway. Conversely, Cripto regulates the metabolic reprogramming that occurs in the transition from ESCs to EpiSCs, at least in part through the Nodal/Smad2/Pgc-1b axis. Finally, Cripto/Nodal/Smad2 sustains mouse EpiSC/hESC self-renewal and prevents transdifferentiation towards the trophoblast lineage, by repressing BMP/Smad1-5 signalling. Our findings place Cripto at the interface of the mouse and human pluripotency networks, and provide unprecedented evidence that it restricts ESC differentiation potential towards embryonic tissue.

homogeneous cell colonies with a typical flat morphology, Cripto BP-treated EpiSCs colonies progressively lose their characteristic morphological appearance and become differentiated (Fig. 8b). Accordingly, EpiSCs markers were strongly downregulated, whereas expression of the neuronal differentiation marker β III-tubulin was induced (Fig. 8c). Interestingly, *Cdx2* expression was also strongly induced in BP-treated EpiSCs and the majority of *Cdx2*⁺ cells did not express Brachyury (Fig. 8b,c). Together, these findings indicated that Cripto-dependent Nodal signalling is required to sustain EpiSCs pluripotency/self-renewal and prompted us to extend the analysis to hESCs, which are similar to mEpiSCs. Consistent with what was previously reported⁴³, surface CRIPTO protein was highly expressed in hESCs (Supplementary Fig. 5a). To investigate whether CRIPTO is required to maintain hESC pluripotency, we evaluated the effect of blocking CRIPTO signalling. To this end, hESCs were grown on feeders in the presence of either Cripto BP or CP and analysed after two passages (Fig. 8d). Similar to that observed in F/A EpiSCs, SMAD2 phosphorylation was strongly inhibited in Cripto BP-hESCs, already after the first passage in culture, thereby proving the activity of the BP (Fig. 8e). Interestingly, although CP-hESCs maintained their undifferentiated morphology, Cripto BP-hESC colonies appeared heterogeneous and clearly showed areas of differentiated cells that stained positive for CDX2 (Fig. 8f). Consistent with the idea that SMAD2 represses autocrine BMP signalling, which in turn induces CDX2-positive trophoblast committed cells^{37,44}, and in line with our findings on mEpiSCs (Fig. 5d), BMP-dependent

SMAD1/5 phosphorylation was induced in Cripto BP-hESCs (Supplementary Fig. 5b). To rule out the possibility that these cells may represent a subpopulation of mesodermal cells that go through a BRACHYURY-positive state⁴⁵, we performed double CDX2/BRACHYURY staining and found only few BRACHYURY/CDX2 double-positive cells (Supplementary Fig. 5c). We thus went on and evaluated the biological effect of Cripto BP on hESC self-renewal. Remarkably, we found a dramatic decrease of the colony-formation capacity of Cripto BP-hESCs compared with CP in semisolid cultures (Fig. 8g). Moreover, Cripto BP-hESC colonies were significantly smaller in size (Fig. 8g), thus indicating that blocking CRIPTO signalling affected hESC self-renewal potential. Furthermore, poly (ADP-ribose) polymerase (PARP) activation was detected in Cripto BP-hESCs, suggesting increased cell death (Supplementary Fig. 5d). All together, these data point to a key role of CRIPTO signalling in sustaining hESC pluripotency and self-renewal, and preventing their transdifferentiation into extraembryonic derivatives. To validate the findings obtained by pharmacological inhibition of CRIPTO, we assessed the effect of *CRIPTO* silencing using lentiviral vectors containing two different short hairpin (shRNA) sequences targeting the 3'-untranslated region and the coding sequence of *CRIPTO*, respectively²³. Silencing of *CRIPTO* by lentiviral shRNA knockdown (KD) resulted in a strong reduction of CRIPTO protein expression (Supplementary Fig. 5e). CRIPTO KD and Control hESCs were then subjected to a matrigel clonogenic assay and the resulting colonies were analysed by immunofluorescence for the pluripotency markers OCT4 and NANOG, and AP staining. The quantification analysis of either OCT4-, NANOG- or AP-positive colonies showed a dramatic reduction of colony number in both *CRIPTO* KD hESC clones, which were also significantly smaller in size compared with Control (Fig. 8h,i and Supplementary Fig. 5f-h), thus providing evidence that CRIPTO KD strongly affected the clonogenic potential of hESCs.

All together, these findings indicate that CRIPTO sustains hESC self-renewal, at least in part, through activation of NODAL signalling.

Discussion

This work shows that the membrane protein Cripto is essential for mouse EpiSC and hESC pluripotency, and provides mechanistic insights into how the extracellular environment controls early cell-fate decisions in the embryo (Fig. 9). We demonstrate that Cripto is one of the earliest EPI markers and provide unprecedented evidence that it plays a pivotal functional role in the acquisition/maintenance of mouse and human pluripotency. Consistent with the salt-and-pepper distribution of Cripto within the ICM of the pre-implantation blastocyst, which underlies the emergence of EPI and PrE lineages¹, surface Cripto protein is heterogeneous and highly dynamic in serum/LIF ESCs and positively correlates with the expression of the pluripotency factors. Heterogeneity and fluctuations in the expression of pluripotency markers in ESCs may be considered as culture-induced perturbations and their relevance to pluripotency and cell-fate decision is still a matter of debates⁴⁶. Our *in vivo* and *in vitro* results challenge the idea of a functional role of Cripto heterogeneity in pluripotency. Indeed, *Cripto* genetic ablation facilitates the exit from naive pluripotency *in vitro* and affects both the efficiency and latency of ESC-derived teratomas formation. At mechanistic level, Cripto regulates mouse ESC self-renewal by positively modulating the canonical Wnt/ β -catenin pathway. Despite the fact that Cripto deficiency facilitates the exit from naive pluripotency in FBS/LIF ESCs, this effect does not accelerate the transition to the primed state, but

rather affects the conversion of ESCs to EpiSCs. Remarkably, this *Cripto* KO mutant phenotype is due to impaired metabolic switch from OXPHOS to aerobic glycolysis, which is required to convert ESCs to EpiSCs³¹. Indeed, while mouse ESCs are bivalent in their energy production, dynamically switching from glycolysis to mitochondrial respiration, both mEpiSCs and hESCs are highly glycolytic³¹. Our findings point to a functional link between *Cripto* and glycolytic metabolism *in vitro* and raise the intriguing possibility that it may play a similar role *in vivo*. Indeed, it has been recently proposed that Activin/Nodal controls the proper metabolic switch in early embryo by repressing mitochondrial activity through inhibition of PGC-1 β ³¹. In line with this idea and according to the key role of *Cripto* as Nodal coreceptor, *Pgc-1 β* is upregulated in F/A *Cripto* KO cells and its downregulation is able to increase lactate production. Although additional experiments are needed to get further insights into the mechanism, our data suggest that *Cripto* controls the metabolic reprogramming, at least in part, through the Nodal/*Pgc-1 β* axis. Consistent with the idea that this metabolic switch is a key event in ESC→EpiSC transition³¹, we demonstrate that *Cripto* is required to generate/maintain FGF/Activin (F/A) EpiSCs. Indeed, we cannot rule out the possibility that *Cripto* KO F/A EpiSCs form but rapidly and continuously get lost from the cultures and/or differentiate. However, quite unexpectedly, we find that *Cripto* deficiency skews ESC differentiation towards TE *in vitro*. Several data support this intriguing idea. TE markers are induced at RNA and protein level; specifically, *Cdx2* significantly increased in F/A *Cripto* KO cells and does not co-localize with Brachyury, thus ruling out the possibility that *Cdx2*-expressing cells identify posterior mesoderm rather than TE. Furthermore, *Cdx2* does not co-localize with Oct4, consistent with the mutually exclusive expression of these genes during embryogenesis¹⁷. Finally, *Cdx2*-positive cells also express the TE maker *Gata3* (ref. 36). Concomitant to induction of TE markers, expression of the DNA methyltransferase *Dnmt3b* is reduced in F/A *Cripto* KO cells. Interestingly, *Dnmt*-deficient and therefore hypomethylated ESCs/embryos show transdifferentiation to the extraembryonic trophoblast lineage⁴⁷. In line with these findings, morphological and molecular analyses indicate that *Cripto* KO ESCs facilitate the generation of TSCs *in vitro*. Interestingly, several evidence indicate that BMP signalling pathway plays a crucial role in TE differentiation of pluripotent stem cells. Specifically, *Cdx2* expression is directly regulated by the BMP-Smad1/5 pathway⁴⁸, which in turn is repressed by Smad2 (ref. 37). Accordingly, *Cripto* KO inhibits Smad2 activation and conversely induces BMP-dependent Smad1/5 phosphorylation, suggesting that derepression of BMP signalling may account for TE differentiation of F/A-induced *Cripto* KO cells. Most remarkably, according to the idea that *Cripto* deficiency attenuates the normal restriction of mouse ESCs to embryonic lineages, *Cripto* KO ESCs gain the unique property to colonize TE in blastocyst chimera, which is absent in WT ESCs⁴⁰. However, analysis of E6.5 chimeric embryos generated with *Cripto* KO ESCs indicates that these cells efficiently contribute to the embryonic but not to the ectoplacental cone. Although we cannot rule out the possibility that *Cripto* KO ESCs that colonize the TE fail to differentiate properly and thus to efficiently contribute to the trophoblast derivatives, we speculate that a non-cell autonomous activity of *Cripto* in the WT environment may rescue, at least in part, the mutant phenotype. Although further investigations are required to directly address this issue, this hypothesis is consistent with co-culture data showing that non-cell autonomous *Cripto* is able to rescue F/A *Cripto* KO EpiSCs. Intriguingly, to date, no defects in EPI specification/maintenance have been reported in *Cripto*-null mutants that indeed are defective in anterior–posterior axis formation¹⁴. Of note, data in

different mutant context indicate that embryo can tolerate a significant loss of EPI cells¹, thus suggesting that a mild phenotype, such as a smaller EPI, could be rescued by the plasticity of the embryo. In this respect, embryonic development might be less vulnerable than ESC differentiation, as it relies on a more complex network of signals easier to compensate than in ESCs, which may reconcile the apparent discrepancy. Moreover, *Cripto* overlooked function(s) *in vivo* can be also explained by the activity of the epidermal growth factor (EGF)-CFC *Cryptic*. Indeed, *Cryptic* promotes EPI maintenance in the absence of *Cripto* presumably through a non-cell-autonomous activity, as it is only expressed in the visceral endoderm¹⁹. Finally, we speculate that a maternal contribution of *Cripto* may also compensate for the absence of *Cripto* in the early embryo. Accordingly, recent findings report *Cripto* expression in the endometrium during pregnancy, and in the mouse uterus⁴⁹.

All together, our findings have important implications for stem cell biology and for our understanding of the mechanisms that regulate TE segregation from the ICM. First, existing models that Activin/Nodal signalling sustains mEpiSC generation/self-renewal mainly rely on the effect of the small molecule SB431542 (ref. 31), which however is a general antagonist of the TGF β pathway⁵⁰. Here we overcome this limitation and provide evidence that *Cripto*/Nodal/Smad2 is required for mEpiSC generation and self-renewal, and moreover that it is functionally conserved in human pluripotent stem cells. Indeed, consistent with the idea that SMAD2 represses autocrine BMP signalling, which conversely induces TE differentiation in hESCs^{37,44}, pharmacological blocking of *Cripto*/SMAD2 results in increased BMP-dependent SMAD1/5 signalling and TE differentiation.

In summary, our studies provide unprecedented evidence that *Cripto* is a major determinant of mEpiSCs/hESCs pluripotency and add novel important elements to the current model of mammalian pluripotency. Moreover, our findings suggest that *Cripto* may have earlier functions than previously recognized, in the very first lineage decision made by the early embryo.

Methods

Blastocyst collection and whole-mount *in situ* labelling. Embryos were produced by natural matings of CD1 mice. For immunostaining, embryos were fixed with 4% paraformaldehyde (PFA) in PBS overnight at 4 °C, permeabilized with 0.5% Triton X-100 in PBS for 15 min and blocked in 10% FBS in PBS-0.1% Triton for 1 h⁵¹. Fluorescent *in situ* hybridization was described in ref. 52. Experiments were performed in accordance with French and EU guidelines for the care and use of laboratory animals. List of antibodies are in Supplementary Table 1.

Mouse ESC culture and EpiSC generation and maintenance. WT and *Cripto* KO R1 mESCs were cultured in high glucose DMEM medium (Invitrogen, Life Technologies) supplemented with 15% ES-screened FBS (Euroclone), 0.1 mM β -mercaptoethanol (Sigma-Aldrich), 1 mM sodium pyruvate, 2 mM glutamine, 100 U ml⁻¹ penicillin/streptomycin (all from Gibco) and 1,000 U ml⁻¹ recombinant LIF (ESGRO, Millipore)¹⁵. 2i Medium was supplemented with PD0325901 (1 μ M) and CHIR99021 (3 μ M)⁶. Two independent *Cripto* KO ESC clones, that is, DE7 and DE14 (named KO.1 and KO.2), were used throughout the study and were previously described^{15,28}. For stimulation with bFGF, Activin A and Bmp4, 2 \times 10⁶ ESCs were plated in N2B27 on serum-coated dishes and incubated (15') with bFGF (12 ng ml⁻¹, Provitro) or Bmp4 (50 ng ml⁻¹, R&D). Cells were LIF starved (6 h) before stimulation with LIF.

EpiSCs were generated from ESCs as described⁵. Briefly, WT and *Cripto* KO ESCs were seeded at low density (3 \times 10³ cells per cm²) in N2B27 supplemented with Activin A (20 ng ml⁻¹, Invitrogen) and bFGF, and cultured for 6 days.

Cripto BP and CP were dissolved in dimethylsulfoxide and media with peptides were refreshed every other day during ESC to EpiSC transition.

Colony-forming assay. For colony assay, ESCs were trypsinized to obtain a single-cell suspension and plated at low density (100 cells per cm²) in the culture conditions described. After 6 days, colonies were fixed in 4% PFA and stained with crystal violet. Briefly, cells were washed twice with PBS and fixed/stained with a solution of 6% glutaraldehyde and crystal violet. After 30 min at room temperature, cells were carefully washed with tap water and dried for further analysis.

Images were collected on a DMI6000B microscope (Leica Microsystems). The morphological classification (domed/flat) was performed blinded by two investigators. Experiments were performed in triplicate.

Proliferation assays and viable cell count. Cell proliferation was measured using the colorimetric CyQuant cell proliferation assay (Invitrogen), following the manufacturer's instructions. Absorbance was analysed at 480–520 nm, using the Fluoroskan Ascent FL Microplate Fluorometer and Luminometer (Thermo Fisher Scientific, Waltham, MA, USA).

Trophoblast stem cell (TSC) culture. To generate TSCs, ESCs were cultured in TCS medium containing RPMI 1640, 20% FBS (Thermo Scientific), 25 ng ml⁻¹ FGF-4 (Invitrogen), 1 ng ml⁻¹ Heparin (Sigma-Aldrich), 2 mM L-glutamine, 0.1 mM β-mercaptoethanol, 1 mM sodium pyruvate and 50 units per ml¹ Penicillin/Streptomycin (Invitrogen), with 70% feeder conditioned media³⁸. ESCs were plated in TSC medium on gelatin-coated plates in the absence of feeders and passaged every 3 days, and the medium changed every 2 days.

hESC culture and self-renewal assay. The hESC line CSE7 (NIH registration number: 0107) was used throughout the study and was kindly provided by Professor Nissim Benvenisty (The Hebrew University, Israel). Undifferentiated hESCs were maintained in culture either on feeder layer or under feeder-free conditions, using standard procedures. For culture on feeder layer, hESCs were grown in Knockout DMEM (Gibco), supplemented with 20% Knockout Serum Replacement (Gibco), 2 mM glutamine, 1 × non essential amino acids (NEAAs), 100 U ml⁻¹ Penicillin/Streptomycin, 0.1 mM 2-Mercaptoethanol, 10 ng ml⁻¹ bFGF (Gibco). For growth under feeder-free conditions, hESCs were cultured on Matrigel (BD Bioscience)-coated plates, using mTeSR medium (Stem Cell Technologies). hESCs were passaged every 5/6 days. Cells were incubated with TrypleSelect 1 × (Gibco) for 2/3 min and scraped gently with a tip.

For clonogenic assay, hESCs were dissociated with TrypleSelect 1 ×, for 5 min at 37 °C. Dissociated cells were plated on Matrigel and cultured in mTeSR medium in the different conditions. After 6 days in culture, colonies were dissociated and replated at low density in the same conditions. After 4 days, colonies were fixed and stained either with crystal violet (see above for details) or with the Alkaline Phosphatase kit (System Biosciences) to determine AP activity, following the manufacturer's instructions. The colony number and size were analysed, using ImageJ software. Colonies were classified on the basis of the diameter, as follows: micro < 0.2 mm, small 0.2–0.4 mm, medium 0.4–0.7 mm and large > 0.7 mm.

For generating *CRIPTO* KD hESCs, lentiviral pLKO.1 vectors containing either a non-targeting sequence or the shRNA4889 and the shRNA4890 (ref. 23) were used. Cells were plated on Matrigel and cultured in mTeSR medium in the different conditions. Colonies were fixed and stained either with AP (System Biosciences) or Oct4 and Nanog antibodies. The colony number was analysed, using ImageJ software.

Cripto BP and CP were used at 10 and 20 μM in hESC passages and clonogenic assay, respectively.

Flow cytometry and cell sorting. Single-cell suspensions of EpiSCs and hESCs were obtained using either trypsin-EDTA or TrypleSelect 1 × (Gibco), fixed, stained with the appropriated primary and secondary antibodies according to the manufacturer's protocols and were either analysed with a FACS Canto (Becton Dickinson) or sorted with a FACS Aria (Becton Dickinson).

Western blotting. Whole-cell lysates were prepared with ice-cold immunoprecipitation assay (RIPA) lysis buffer. For β-catenin localization, subcellular fractionation was performed as described⁵³. Detection was performed with ECL reagents (Amersham Biosciences). Densitometric analysis was carried out using the software GelEval 1.35. List of antibodies is in Supplementary Table 1. Full blots are in Supplementary Fig. 6.

Immunohistochemistry. Samples were processed with the standard streptavidin-biotin-immunoperoxidase method (DAKO Universal Kit, DAKO Corp., Carpinteria, CA, USA). Diaminobenzidine was used as the final chromogen and haematoxylin as the nuclear counter stain. Details and list of antibodies are in Supplementary Table 1.

Immunofluorescence and cytospin samples preparation. Cells were fixed (4% PFA) and permeabilized (0.1% Triton X-100), where necessary, at room temperature. After incubation with primary antibodies, cells were incubated (1 h) with the appropriate secondary antibodies (Alexa Fluor 488, 594 1:200; Molecular Probes). For preparation of cytospin samples, cells (1–1.5 × 10⁴) were dissociated with accutase for 5 min at 37 °C and resuspended in 15% FBS/1 × PBS. Samples were centrifuged at 900 r.p.m. for 15 min onto glass slides (2 spots, 1 × 10⁵ cells each) using a Thermo Shandon CytoSpin 4, Thermo Fisher Scientific). Specimens were directly analysed or fixed for further analysis. Details and list of antibodies are in Supplementary Table 1.

RNA extraction and quantitative reverse transcriptase-PCR. Total RNAs were isolated using RNeasy mini kit and reverse transcribed using QuantiTect Reverse Transcription kit (Qiagen). qPCR was performed using SYBR Green PCR master mix (FluoCycle II SYBR, EuroClone). Details and list of primers are in Supplementary Table 2.

Whole-genome expression analysis. RNA-seq was performed at the Institute for Applied Genomics using the Illumina HiSeq 2500 platform (<http://www.igatechnology.com/>). Gene expression analysis was obtained by counting reads mapped on gene features, by using *htseq-count*⁵⁴ and the statistical analysis was performed by using RNASeqGUI⁵⁵. In detail, paired-end fastq files were first aligned on the mouse genome version mm9 (downloaded from <http://hgdownload.cse.ucsc.edu/goldenPath/mm9/chromosomes>) by using TopHat2 (version tophat-2.0.13)⁵⁶ with -G option and using as gene annotation file the release 67 of NCBI37, downloaded from ftp://ftp.ensembl.org/pub/release-67/gtf/mus_musculus/ repository; all other parameters were set as default. HTSeq⁵⁴ (version 0.6.1p1) was used to obtain raw counts on intersection non-empty mode by using the same gene annotation file. Next, raw counts were processed by using the RNSeqGUI (version 0.99.3)⁵⁵. In particular, the 'normalize.quantiles' normalization function of the preprocessCore R package (Bolstad B.M. preprocessCore: A collection of pre-processing functions; version preprocessCore_1.28.0) was used to normalize the gene expression values. Those genes with low expressions in all samples were filtered out by using the 'Proportion test' of NOISeq⁵⁷ (version NOISeq_2.8.0). In the filtering step we used cpm = 1. Finally, we used full quantile-normalized and filtered counts to perform differentially expression analysis. For such purpose, we used NOISeq (version 2.8.0) with posterior probability set to 0.95. As NOISeq test has a stochastic component, for each comparison we launched NOISeq ten times, each time setting a different seed. Hence, for each gene we calculated the mean of the ten posterior probabilities obtained so far. We considered a gene as differentially expressed across the samples if the mean of the ten posterior probabilities was ≥ 0.95. A sketch of the code used for carrying out the statistical analysis is given in Supplementary Data 4. Despite the fact that we have applied a stringent procedure, the absence of replicates does not allow us to define significance in a rigorous statistical sense. Yet, the RNA-Seq results were validated by independent experiments.

Genes were classified according to their known or predicted biological functions based on GO terms (DAVID Bioinformatics Resources; <http://david.abcc.ncifcrf.gov>).

Luciferase reporter assay. ESCs were transfected with the Super8xTOPFlash and the *Renilla*-TK mutant plasmids using Lipofectamine, according to the manufacturer's protocol (Invitrogen). At 24 h after transfection, ESCs were treated with Wnt3a (R&D Systems, 5–50 ng ml⁻¹) for 24 h⁵⁸, and Luciferase activity was measured by using a dual Luciferase assay kit (Promega) according to the manufacturer's instructions.

Lactate activity assay. Lactate was measured using the colorimetric L-Lactate Assay Kit (Abcam, Cambridge, MA, USA; ab65331) according to the manufacturer's instructions. Data were normalized to total cell number.

Teratoma assay. ESCs were trypsinized into single-cell suspension and resuspended in PBS. ESCs (3 × 10⁶) were injected subcutaneously into hind limbs of severe combined immunodeficiency mice. Teratomas were collected, fixed in 4% PFA, sectioned and stained with haematoxylin/eosin or subjected to immunohistochemistry for the histological analysis.

Experiments were done in accordance to the law on animal experimentation (article 7; D.L. 116/92) under the Animal Protocol approved by the Italian Ministry of Health.

GFP-labelled ESCs and TE lineage contribution. GFP was inserted in both WT and Cripto KO ESCs at the Rosa26 locus by using the R26P-SA-EGFPpuro plasmid (Addgene). Ten days after transfection, puromycin-selected clones were verified for correct self-renewal and differentiation properties.

Chimeras were obtained by injecting WT and Cripto KO GFP-labelled ESCs (13–16) into 4- to 8-cell-stage embryos using standard techniques. Morulas were incubated 48 h in KSOM (Chemical International) and observed under the confocal microscope (Zeiss LSM700). Chimeric mouse generation was performed by morula injection of WT and Cripto KO GFP-labelled ESCs. Resultant embryos were cultured for 48 h *in vitro* and implanted by uterus transfer into pseudopregnant foster mothers using standard methods. Pregnant mice were killed at day E6.5 and whole embryos were photographed with ApoTome fluorescence microscope. Experiments were done in accordance to the law on animal experimentation (article 7; D.L. 116/92) under the Animal Protocol approved by the Italian Ministry of Health.

Statistical analysis. Statistical significance was determined by a two-tailed paired Student's *t*-test. *P*-values <0.05 were considered as statistically significant. Error bars represent s.e.m.

Data availability. Sequence data that support the findings of this study have been deposited to the GEO database with the accession code GSE79796. The authors confirm that all other data appears in the article and Supplementary Information.

References

- Artus, J. & Chazaud, C. A close look at the mammalian blastocyst: epiblast and primitive endoderm formation. *Cell. Mol. Life Sci.* **71**, 3327–3338 (2014).
- Bedzhov, I., Graham, S. J., Leung, C. Y. & Zernicka-Goetz, M. Developmental plasticity, cell fate specification and morphogenesis in the early mouse embryo. *Phil. Trans. R. Soc. Lond. B Biol. Sci.* **369** (2014).
- Nichols, J. & Smith, A. Naive and primed pluripotent states. *Cell Stem Cell* **4**, 487–492 (2009).
- Brons, I. G. *et al.* Derivation of pluripotent epiblast stem cells from mammalian embryos. *Nature* **448**, 191–195 (2007).
- Tesar, P. J. *et al.* New cell lines from mouse epiblast share defining features with human embryonic stem cells. *Nature* **448**, 196–199 (2007).
- Guo, G. *et al.* Klf4 reverts developmentally programmed restriction of ground state pluripotency. *Development* **136**, 1063–1069 (2009).
- Hayashi, K., Lopes, S. M., Tang, F. & Surani, M. A. Dynamic equilibrium and heterogeneity of mouse pluripotent stem cells with distinct functional and epigenetic states. *Cell Stem Cell* **3**, 391–401 (2008).
- Toyooka, Y., Shimosato, D., Murakami, K., Takahashi, K. & Niwa, H. Identification and characterization of subpopulations in undifferentiated ES cell culture. *Development* **135**, 909–918 (2008).
- Festuccia, N., Osorno, R., Wilson, V. & Chambers, I. The role of pluripotency gene regulatory network components in mediating transitions between pluripotent cell states. *Curr. Opin. Genet. Dev.* **23**, 504–511 (2013).
- Comes, S. *et al.* L-Proline induces a mesenchymal-like invasive program in embryonic stem cells by remodeling H3K9 and H3K36 methylation. *Stem Cell Rep.* **1**, 307–321 (2013).
- Shyh-Chang, N. *et al.* Influence of threonine metabolism on S-adenosylmethionine and histone methylation. *Science* **339**, 222–226 (2012).
- Sternecker, J. L., Reinhardt, P. & Scholer, H. R. Investigating human disease using stem cell models. *Nat. Rev. Genet.* **15**, 625–639 (2014).
- Nagaoka, T. *et al.* An evolving web of signaling networks regulated by Cripto-1. *Growth Factors* **30**, 13–21 (2012).
- Ding, J. *et al.* Cripto is required for correct orientation of the anterior-posterior axis in the mouse embryo. *Nature* **395**, 702–707 (1998).
- Parisi, S. *et al.* Nodal-dependent Cripto signaling promotes cardiomyogenesis and redirects the neural fate of embryonic stem cells. *J. Cell Biol.* **163**, 303–314 (2003).
- Mallon, B. S. *et al.* StemCellDB: the human pluripotent stem cell database at the National Institutes of Health. *Stem Cell Res.* **10**, 57–66 (2013).
- Strumpf, D. *et al.* Cdx2 is required for correct cell fate specification and differentiation of trophectoderm in the mouse blastocyst. *Development* **132**, 2093–2102 (2005).
- Takaoka, K. *et al.* The mouse embryo autonomously acquires anterior-posterior polarity at implantation. *Dev. Cell* **10**, 451–459 (2006).
- Chu, J. & Shen, M. M. Functional redundancy of EGF-CFC genes in epiblast and extraembryonic patterning during early mouse embryogenesis. *Dev. Biol.* **342**, 63–73 (2010).
- Minchiotti, G. *et al.* Membrane-anchorage of Cripto protein by glycosylphosphatidylinositol and its distribution during early mouse development. *Mech. Dev.* **90**, 133–142 (2000).
- Boroviak, T., Loos, R., Bertone, P., Smith, A. & Nichols, J. The ability of inner-cell-mass cells to self-renew as embryonic stem cells is acquired following epiblast specification. *Nat. Cell Biol.* **16**, 516–528 (2014).
- Torres-Padilla, M. E. & Chambers, I. Transcription factor heterogeneity in pluripotent stem cells: a stochastic advantage. *Development* **141**, 2173–2181 (2014).
- Francescangeli, F. *et al.* Dynamic regulation of the cancer stem cell compartment by Cripto-1 in colorectal cancer. *Cell Death Differ.* **22**, 1700–1713 (2015).
- Loying, P., Manhas, J., Sen, S. & Bose, B. Autoregulation and heterogeneity in expression of human Cripto-1. *PLoS One* **10**, e0116748 (2015).
- ten Berge, D. *et al.* Embryonic stem cells require Wnt proteins to prevent differentiation to epiblast stem cells. *Nat. Cell Biol.* **13**, 1070–1075 (2011).
- Nagaoka, T. *et al.* Cripto-1 enhances the canonical Wnt/beta-catenin signaling pathway by binding to LRP5 and LRP6 co-receptors. *Cell. Signal.* **25**, 178–189 (2013).
- Geula, S. *et al.* Stem cells. m6A mRNA methylation facilitates resolution of naive pluripotency toward differentiation. *Science* **347**, 1002–1006 (2015).
- Xu, C., Liguori, G., Adamson, E. D. & Persico, M. G. Specific arrest of cardiogenesis in cultured embryonic stem cells lacking Cripto-1. *Dev. Biol.* **196**, 237–247 (1998).
- Ben-David, U., Nudel, N. & Benvenisty, N. Immunologic and chemical targeting of the tight-junction protein Claudin-6 eliminates tumorigenic human pluripotent stem cells. *Nat. Commun.* **4**, 1992 (2013).
- Bernemann, C. *et al.* Distinct developmental ground states of epiblast stem cell lines determine different pluripotency features. *Stem Cells* **29**, 1496–1503 (2011).
- Zhou, W. *et al.* HIF1alpha induced switch from bivalent to exclusively glycolytic metabolism during ESC-to-EpiSC/hESC transition. *EMBO J.* **31**, 2103–2116 (2012).
- Chappell, J. B. & Greville, G. D. Effects of oligomycin on respiration and swelling of isolated liver mitochondria. *Nature* **190**, 502–504 (1961).
- Li, L. *et al.* Activin signaling: effects on body composition and mitochondrial energy metabolism. *Endocrinology* **150**, 3521–3529 (2009).
- Minchiotti, G. Nodal-dependant Cripto signaling in ES cells: from stem cells to tumor biology. *Oncogene* **24**, 5668–5675 (2005).
- Lewis, S. L. & Tam, P. P. Definitive endoderm of the mouse embryo: formation, cell fates, and morphogenetic function. *Dev. Dyn.* **235**, 2315–2329 (2006).
- Ralston, A. *et al.* Gata3 regulates trophoblast development downstream of Tead4 and in parallel to Cdx2. *Development* **137**, 395–403 (2010).
- Sakaki-Yumoto, M., Liu, J., Ramalho-Santos, M., Yoshida, N. & Derynck, R. Smad2 is essential for maintenance of the human and mouse primed pluripotent stem cell state. *J. Biol. Chem.* **288**, 18546–18560 (2013).
- Koh, K. P. *et al.* Tet1 and Tet2 regulate 5-hydroxymethylcytosine production and cell lineage specification in mouse embryonic stem cells. *Cell Stem Cell* **8**, 200–213 (2011).
- Guzman-Ayala, M., Ben-Haim, N., Beck, S. & Constam, D. B. Nodal protein processing and fibroblast growth factor 4 synergize to maintain a trophoblast stem cell microenvironment. *Proc. Natl Acad. Sci. USA* **101**, 15656–15660 (2004).
- Rossant, J. Stem cells from the mammalian blastocyst. *Stem Cells* **19**, 477–482 (2001).
- Chu, J. *et al.* Non-cell-autonomous role for Cripto in axial midline formation during vertebrate embryogenesis. *Development* **132**, 5539–5551 (2005).
- Lonardo, E. *et al.* A small synthetic cripto blocking Peptide improves neural induction, dopaminergic differentiation, and functional integration of mouse embryonic stem cells in a rat model of Parkinson's disease. *Stem Cells* **28**, 1326–1337 (2010).
- Hough, S. R., Laslett, A. L., Grimmond, S. B., Kolle, G. & Pera, M. F. A continuum of cell states spans pluripotency and lineage commitment in human embryonic stem cells. *PLoS ONE* **4**, e7708 (2009).
- Kurek, D. *et al.* Endogenous WNT signals mediate BMP-induced and spontaneous differentiation of epiblast stem cells and human embryonic stem cells. *Stem Cell Rep.* **4**, 114–128 (2015).
- Bernardo, A. S. *et al.* BRACHYURY and CDX2 mediate BMP-induced differentiation of human and mouse pluripotent stem cells into embryonic and extraembryonic lineages. *Cell Stem Cell* **9**, 144–155 (2011).
- Smith, A. Nanog heterogeneity: tilting at windmills? *Cell Stem Cell* **13**, 6–7 (2013).
- Ng, R. K. *et al.* Epigenetic restriction of embryonic cell lineage fate by methylation of Elf5. *Nat. Cell Biol.* **10**, 1280–1290 (2008).
- Hayashi, Y. *et al.* BMP4 induction of trophoblast from mouse embryonic stem cells in defined culture conditions on laminin. *In vitro cellular & developmental biology. Animal* **46**, 416–430 (2010).
- Park, C. B. & Dufort, D. Nodal expression in the uterus of the mouse is regulated by the embryo and correlates with implantation. *Biol. Reprod.* **84**, 1103–1110 (2011).
- Inman, G. J. *et al.* SB-431542 is a potent and specific inhibitor of transforming growth factor-beta superfamily type I activin receptor-like kinase (ALK) receptors ALK4, ALK5, and ALK7. *Mol. Pharmacol.* **62**, 65–74 (2002).
- Chazaud, C., Yamanaka, Y., Pawson, T. & Rossant, J. Early lineage segregation between epiblast and primitive endoderm in mouse blastocysts through the Grb2-MAPK pathway. *Dev. Cell* **10**, 615–624 (2006).
- Gasnier, M., Dennis, C., Vauurs-Barriere, C. & Chazaud, C. Fluorescent mRNA labeling through cytoplasmic FISH. *Nat. Protoc.* **8**, 2538–2547 (2013).
- Kim, H. *et al.* Modulation of beta-catenin function maintains mouse epiblast stem cell and human embryonic stem cell self-renewal. *Nat. Commun.* **4**, 2403 (2013).
- Anders, S., Pyl, P. T. & Huber, W. HTSeq—a Python framework to work with high-throughput sequencing data. *Bioinformatics* **31**, 166–169 (2015).
- Russo, F. & Angelini, C. RNASeqGUI: a GUI for analysing RNA-Seq data. *Bioinformatics* **30**, 2514–2516 (2014).
- Kim, D. *et al.* TopHat2: accurate alignment of transcriptomes in the presence of insertions, deletions and gene fusions. *Genome Biol.* **14**, R36 (2013).
- Tarazona, S., Garcia-Alcalde, F., Dopazo, J., Ferrer, A. & Conesa, A. Differential expression in RNA-seq: a matter of depth. *Genome Res.* **21**, 2213–2223 (2011).
- Fico, A. *et al.* Modulating Glypican4 suppresses tumorigenicity of embryonic stem cells while preserving self-renewal and pluripotency. *Stem Cells* **30**, 1863–1874 (2012).

Acknowledgements

We thank the Animal House, Integrated Microscopy and FACS Facilities of IGB-CNR, and Marinella Pirozzi and the Bioimaging Facility of IBP-CNR, Naples. We are grateful to Professor Nissim Benvenisty for kindly providing hESCs. Gabriele Di Napoli is acknowledged for excellent technical assistance. This work is supported by AIRC (11599 to G.M. and 15749 to A.Z.), European Community's Seventh Framework Programme in the project ENDOSTEM, Epigenomics Flagship Project MIUR-CNR (to G.M. and C.A.), Italian Ministry of Education-University-Research (PRIN and PON Cluster IRMI) to G.M. E.J.P. is supported by Medical Research in Italy (RBNE08HM7T-003). C.C. is supported by ANR (PrEpiSpec) and ARC (PJA 20131200380) grants.

Author contributions

A. Fiorenzano, E.P., C.D.A., D.A., C.B., G.A., C.C. and A.F. performed the experiments. A. Fiorenzano, C.D.A., C.C., E.J.P., A.F. and G.M. planned and designed the experiments and analysed the data. F.R. performed bioinformatics analyses of expression data. C.A. supervised bioinformatics analyses. M.B., F.F. and A.Z. contributed reagents/analysis tools/technical expertise. A.F. and G.M. conceived the work. C.C., E.J.P. and A.F. gave conceptual advice and edited the manuscript. G.M. wrote the manuscript. All authors reviewed and approved the manuscript.

Additional information

Supplementary Information accompanies this paper at <http://www.nature.com/naturecommunications>

Competing financial interests: The authors declare no competing financial interests.

Reprints and permission information is available online at <http://npg.nature.com/reprintsandpermissions/>

How to cite this article: Fiorenzano, A. *et al.* Cripto is essential to capture mouse epiblast stem cell and human embryonic stem cell pluripotency. *Nat. Commun.* 7:12589 doi: 10.1038/ncomms12589 (2016).



This work is licensed under a Creative Commons Attribution 4.0 International License. The images or other third party material in this article are included in the article's Creative Commons license, unless indicated otherwise in the credit line; if the material is not included under the Creative Commons license, users will need to obtain permission from the license holder to reproduce the material. To view a copy of this license, visit <http://creativecommons.org/licenses/by/4.0/>

© The Author(s) 2016